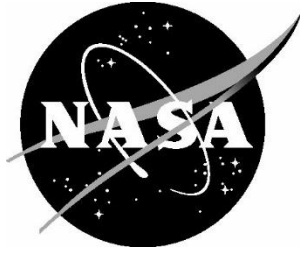


NASA/TM- 20250000022



# Physics-Based Modeling and Simulation of Self-Reacting Friction Stir Welding Using Computational Fluid Dynamics

*Paul W. C. Northrop*

*CFD Research Corporation/Amentum Space Exploration Division/ESSCA  
Huntsville, Alabama*

*J. Vernon Cole*

*CFD Research Corporation, Huntsville, Alabama*

---

January 2025

# NASA STI Program Report Series

Since its founding, NASA has been dedicated to the advancement of aeronautics and space science. The NASA scientific and technical information (STI) program plays a key part in helping NASA maintain this important role.

The NASA STI program operates under the auspices of the Agency Chief Information Officer. It collects, organizes, provides for archiving, and disseminates NASA's STI. The NASA STI program provides access to the NTRS Registered and its public interface, the NASA Technical Reports Server, thus providing one of the largest collections of aeronautical and space science STI in the world. Results are published in both non-NASA channels and by NASA in the NASA STI Report Series, which includes the following report types:

- **TECHNICAL PUBLICATION.** Reports of completed research or a major significant phase of research that present the results of NASA Programs and include extensive data or theoretical analysis. Includes compilations of significant scientific and technical data and information deemed to be of continuing reference value. NASA counterpart of peer-reviewed formal professional papers but has less stringent limitations on manuscript length and extent of graphic presentations.
- **TECHNICAL MEMORANDUM.** Scientific and technical findings that are preliminary or of specialized interest, e.g., quick release reports, working papers, and bibliographies that contain minimal annotation. Does not contain extensive analysis.
- **CONTRACTOR REPORT.** Scientific and technical findings by NASA-sponsored contractors and grantees.

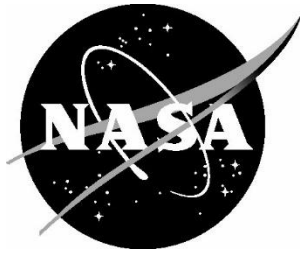
- **CONFERENCE PUBLICATION.** Collected papers from scientific and technical conferences, symposia, seminars, or other meetings sponsored or co-sponsored by NASA.
- **SPECIAL PUBLICATION.** Scientific, technical, or historical information from NASA programs, projects, and missions, often concerned with subjects having substantial public interest.
- **TECHNICAL TRANSLATION.** English-language translations of foreign scientific and technical material pertinent to NASA's mission.

Specialized services also include organizing and publishing research results, distributing specialized research announcements and feeds, providing information desk and personal search support, and enabling data exchange services.

For more information about the NASA STI program, see the following:

- Access the NASA STI program home page at <http://www.sti.nasa.gov>

NASA/TM– 20250000022



# Physics-Based Modeling and Simulation of Self-Reacting Friction Stir Welding Using Computational Fluid Dynamics

*Paul W. C. Northrop  
CFD Research Corporation/Amentum Space Exploration Division/ESSCA  
Huntsville, Alabama*

*J. Vernon Cole  
CFD Research Corporation, Huntsville, Alabama*

---

January 2025

## Acknowledgements

The authors would like to thank Ilana Lu and Dr. Robert Amaro from the Welding and Manufacturing Team at NASA Marshall Space Flight Center for their support. Their expert guidance was instrumental in informing the direction of the SR-FSW model development and has been greatly appreciated. We also acknowledge Dr. Joshua Stuckner (NASA Glenn Research Center) and Dr. Anthony Reynolds (University of South Carolina) for their discussions that improved the quality of this manuscript.

The use of trademarks or names of manufacturers in this report is for accurate reporting and does not constitute an official endorsement, either expressed or implied, of such products or manufacturers by the National Aeronautics and Space Administration.

Available from:

NASA STI Program / Mail Stop 050  
NASA Langley Research Center  
Hampton, VA 23681-2199

## TABLE OF CONTENTS

1	Abstract.....	11
2	Introduction .....	11
3	Motivation of CFD-Based SR-FSW Modeling.....	12
4	CFD Modeling Overview.....	13
4.1	Model Domain .....	13
4.2	Governing Equations.....	14
4.2.1	Flow Model .....	14
4.2.2	Thermal Model.....	15
4.3	Fundamental Outputs .....	16
5	CFD Model Details.....	17
5.1	Flow stress .....	17
5.2	Friction Model.....	18
5.3	Volumetric Plastic Heating.....	18
5.4	Stick Slip Model.....	19
5.5	Thermal Parameters .....	20
5.6	Material Transition.....	20
5.7	Derived Variables .....	21
5.7.1	User-Defined Memory (UDM) Variables.....	21
5.7.2	User Defined Scalar (UDS) Variables.....	22
5.7.3	Discrete Phase Model .....	24
5.8	Computational Considerations .....	24
5.8.1	Accuracy / Meshing, Discretization, and Solver Options .....	25
5.8.2	Stability / Relaxation Factors .....	26
5.8.3	Mesh Adaptation .....	29
6	Calculated Simulation Outputs .....	30
6.1	Tracers.....	30
6.2	Mixing Maps.....	32
6.3	Cross sections.....	34
6.4	Shoulder Interface .....	35
6.5	Output Parameters .....	36
7	Conclusions .....	37
8	Appendix: Flow Stress Parameterization .....	39
9	References.....	41

## LIST OF FIGURES

Figure 1: Schematic of the Model Domain for Self-Reacting Friction Stir Welding.....	14
Figure 2: Material streamlines generated using the physics-based computational model colored by temperature as it is welded. ....	16
Figure 3: (a) Initial mesh near the tool/workpiece interface. (b) Mesh after one level of refinement near the pin tool.....	29
Figure 4: Numerical tracer studies of planes orientated parallel to the weld surface (a), parallel to the weld seam (b), and parallel to the transverse plane (c). The blue lines on the tool schematic indicate the initial orientation of the tracer material. For (a) and (b) the view is orientated in the direction of the weld. For (c), the view is from the top and the various tracers show results at different depths from the crown surface.....	31
Figure 5: Scattered tracer experiment showing how material is transported transverse to the weld direction. The tracers' origin locations (Red +) and final locations (Blue x) are indicated. The figure orientation is such that the weld is progressing into the page. ....	32
Figure 6: Streamlines colored by initial material (Left). Contours on weld seam surface colored by initial material (Right). ....	33
Figure 7: Weld cross section showing origin panel of material using the DPM/Lagrangian (Left) and UDS/Eularian (Right) analysis.....	33
Figure 8: Weld cross section showing origin panel of material with a welding offset (Left) and showing final material transport of an inserted shim between the workpiece panels (Right). ....	34
Figure 9: Example contour plots obtained by tracing streamlines to weld exit and colored by: maximum temperature (Top Left), maximum strain rate (Top Right), material residence time (Bottom Left), and simulated Vickers' hardness using the model by Shercliff et al. [29] (Bottom Right). ....	34
Figure 10: Example results at the crown/workpiece interface showing the (a) temperature, (b) material velocity, and (c) local slip. ....	35
Figure 11: Simulated average temperature at tool interface as a function of operational parameters (RPM and IPM).....	37

## LIST OF TABLES

Table 1: Example List of UDM Variables Defined in the SR-FSW Physics-Based Model .....	22
Table 2: Example List of UDS Variables Defined in the SR-FSW Physics-Based Model.....	23
Table 3: Example List of DPM Variables Defined in the SR-FSW Physics-Based Model.....	24
Table 4: Solver options for the variables considered in the SR-FSW model.....	26
Table 5: Output variables and the mathematical operation applied to each streamline. ....	34
Table 6: Example output parameters from SR-FSW simulations.....	37

## ACRONYM LIST

CFD	Computational Fluid Dynamics
DPM	Discrete Phase Model
FSW	Friction Stir Welding
HAZ	Heat Affected Zone
SLS	Space Launch System
SR-FSW	Self-Reacting Friction Stir Welding
TMAZ	Thermo-Mechanically Affected Zone
UDF	User-Defined Function
UDM	User-Defined Memory
UDS	User-Defined Scalar

## VARIABLE LIST

$c$	Pin handedness
$c_p$	Material specific heat
$f_T$	Fraction of nugget transition due to maximum temperature (empirical)
$f_{ZH}$	Fraction of nugget transition due to maximum Zener-Holloman parameter (empirical)
$H$	Specific Enthalpy
$K$	Shoulder scroll pitch
$k_{pin}$	Pin thread pitch
$k$	Thermal Conductivity
$P$	Pressure
$\dot{Q}_{plas}$	Volumetric heat generation due to plastic heating.
$Q$	Activation energy of flow stress
$\dot{Q}_{fric}$	Heat Generation due to friction
$T$	Temperature
$T_{max}$	Maximum temperature experienced by material parcel
$T_{trans}$	Temperature for transition to nugget properties
$\Delta T_{trans}$	Width of temperature transition to nugget properties
$\vec{u}$	Velocity vector
$\vec{v}_{weld}$	Weld speed
$Z$	Zener-Holloman parameter (temperature compensated strain rate)
$Z_{H,max}$	Maximum Zener-Holloman parameter value experienced by material parcel
$Z_{H,trans}$	Zener-Holloman value for transition to nugget properties
$\Delta Z_{H,trans}$	Width of Zener-Holloman transition to nugget properties

## VARIABLE LIST (CONTINUED)

$\alpha, A, n$	Sheppard-Wright Parameters
$\beta_{scroll}$	Shoulder scroll engagement factor
$\delta$	Slip at shoulder
$\delta_{pin}$	Slip at pin
$\epsilon$	Material emissivity
$\dot{\epsilon}$	Strain rate
$\mu$	Effective viscosity
$\mu_{FC}$	Coulomb friction coefficient
$\phi$	Generic placeholder variable or parameter
$\rho$	Density
$\sigma$	Stefan-Boltzmann Constant, Flow Stress
$\tau_{fric}$	Frictional shear stress
$\tau_{yield}$	Shear yield stress
$\vec{\omega}$	Tool angular velocity vector

## 1 ABSTRACT

A physics-based model was developed to simulate the behavior of material in a self-reacting friction stir welding (SR-FSW) process for the joining of metals. This steady-state model builds upon fundamental computational fluid dynamic (CFD) principles within Ansys Fluent to solve the discretized equations. The effective viscosity is calculated using a viscoplastic model using a Sheppard-Wright formulation of flow stress. Numerous advancements have been made in the incorporated physics including (1) temperature-dependent material properties; (2) locally adaptable flow and thermal boundary conditions; and (3) adapting material properties in nugget in response to microstructural changes. Simulation strategies to accelerate computation and improve numerical stability include adapting the mesh refinement and solver relaxation factors during simulation. The result is a highly robust and computationally efficient model capable of providing the material flow and temperature history across the domain. As material history determines the local microstructure and ultimately weld strength, an accurate and detailed physics-based model has the potential to accelerate SR-FSW process development. The model is highly adaptable to changes in process parameters, tool design, or alloy.

## 2 INTRODUCTION

Friction stir welding (FSW) was developed by The Welding Institute (TWI) in 1991 as a solid-state welding process to produce high strength welds by ensuring that peak temperatures remain below the melting point of the material [1]. In FSW, a rotating threaded pin is forced through a weld seam, plastically deforming and mixing metal from two pieces together to form a bond. A rotating shoulder with a diameter greater than that of the pin contacts the workpiece and provides heat to soften the material around the pin tool and facilitates plasticization while keeping the material contained in the weld. Self-reacting friction stir welding (SR-FSW) is a variant utilizing two shoulders, one on the crown (top) and one on the root (bottom) side, applying a pinching force to the workpiece. SR-FSW can join pieces where a fixed backing plate is not feasible, such as in circumferential welds.

Ultimately, the FSW process results in lower peak temperatures than fusion welding. FSW is suitable for heat treatable aluminum alloys that are difficult to reliably fusion weld yet are popular in the aerospace industry due to their high strength and low weight. As melting does not occur, issues related to resolidification and cooling (e.g., cracking) are reduced and some of the strengthening microstructure (e.g., precipitates) can be preserved. Thus, a properly performed FSW experiences a lower knockdown in mechanical properties than a fusion weld. The stronger weld can reduce the weight of flight hardware by increasing confidence in performance and reducing the required overdesign.

NASA Marshall Space Flight Center (MSFC) has been using FSW since 1995 to avoid some of the issues that arise with the fusion welding of certain aluminum alloys [2] and have incorporated SR-FSW since at least 2003 [3]. Both FSW and SR-FSW are used in the construction of flight hardware for the Space Launch System (SLS) and are finding use in commercial rocket applications.

Despite nearly 30 years of use at MSFC, there is still much to learn about the physical material response during the FSW and SR-FSW process. The tooling makes direct observation of the weld surface impossible

and measuring temperature in the weld is difficult. Thermocouples can be placed on the surface of the workpiece outside of the welding zone but can be moved or damaged if they are in the tool path. Thus, the temperature and flow of the material in the region of most interest (i.e., the weld nugget) must be inferred from post-weld observation (e.g., microstructural analysis) or from measurements some distance away. The inability to perform in situ measurements has limited the fundamental understanding of the physical behavior of the friction welding process. As the temperature and flow characteristics strongly affect the final weld strength, this has arguably limited the development of the technology.

To better understand the FSW behavior, various computational physics-based FSW models have been developed over the years [2] to provide insight into otherwise unobservable processes occurring during the welding process to improve our understanding of the conditions that lead to a successful (or unsuccessful) weld. Increases in available computing power have allowed for simulating more complex models incorporating more physical phenomena. In recent years, physics-based models based on computational fluid dynamic (CFD) principles have been popular [2, 4, 5, 6, 7]. Such CFD-based models enable the tracing of material during the welding process and provide the full localized thermal history of the weld. When combined with advanced numerical techniques for rapid simulation, these models enable quick and cheap exploration of the operational and design parameter space.

This manuscript aims to provide a detailed description of the physics-based model currently available at MSFC for the physics-based simulation of SR-FSW processes. This model has built upon prior efforts described in the literature [8, 6, 9, 10] and has incorporated more detailed physical phenomena and increased computational efficiency. Automated post-processing scripts have been developed to visualize and analyze the generated data. This will facilitate the use of the model to predict weld behavior across a range of operating conditions and tool designs.

### 3 MOTIVATION OF CFD-BASED SR-FSW MODELING

Although SR-FSW has been successfully employed on flight hardware, the internal dynamics of the welding process are not fully understood, especially in the critical weld nugget region. This leads to a time-consuming and expensive process to determine appropriate operating conditions and acceptable tool designs in new applications. For example, developing a new process schedule for a new alloy, or even a different thickness of a well-known alloy, often uses a combination of trial-and-error and expert intuition. Although this approach can (eventually) lead to a robust process, it is slow, may not generalize well to different cases, and relies heavily on experienced personnel. The latter concern can lead to a loss of capabilities when experienced personnel leave the organization. Lessons learned may be lost and tests repeated to regain the lost knowledge. Even worse is learning the wrong lesson, applying an approach that worked in one case to a different application for which it is entirely unsuitable for. The effort required to find and correct such an error could be quite costly.

CFD-based modeling of the SR-FSW process can improve fundamental understanding and shorten development times. Numerical models provide insight into the internal material flow and heat transfer that cannot be directly observed experimentally. Local temperatures and cooling rates in the weld can dramatically affect the weld strength due to aging effects. Flow around the pin tool affects strength by

facilitating material mixing between the two workpieces. However, material entrained in the weld nugget and carried along with the pin tool can be exposed to elevated temperatures for extended times, weakening the material in a manner akin to overaging or resulting in the agglomeration of non-strengthening precipitates that can provide a nucleation site for fracture. Understanding the flow behavior can support the design of pin tools and the selection of operational conditions to mitigate material entrainment and encourage effective bonding. Furthermore, numerical experiments can be performed much more cheaply and much faster than physical experiments. Variations in tool designs or operational conditions can be explored systematically. Simulation results can direct physical experiments to optimize weld performance. A strong physical understanding enables a streamlined approach to process development which can result in stronger and more consistent welds in less time and less material than traditional approaches.

This CFD-based model has been designed to be highly generalizable to different materials and conditions and has been demonstrated on multiple alloys and multiple systems. Although the model must be parameterized for a specific system, the model architecture will not change. Physical parameters such as flow stress and thermal conductivity can be obtained from the literature or dedicated experiments. The tool design and workpiece dimensions define the geometrical parameters. Other empirical parameters (e.g., friction coefficients), can be adjusted to best fit the available data. Ultimately, this results in a highly versatile model adaptable to numerous systems.

## 4 CFD MODELING OVERVIEW

Computational fluid dynamic techniques numerically calculate the momentum transfer within a fluid domain to simulate the flow of a fluid subject to specified boundary conditions. The fluid flow can be coupled with a heat transport model to capture the temperature dynamics of the system. When complete, CFD simulations provide the full fluid flow and temperature profile in the domain, which can provide valuable insight when applied to SR-FSW processes.

SR-FSW is a solid-state process, and melting of the workpiece should not occur, so using fluid dynamic models may seem like an odd choice. However, the high strains that occur during FSW processes mean that computational solid mechanics (CSM) simulation strategies are not suitable in the stir zone. Instead, CFD-based framework simulates the metal workpiece as a viscoplastic fluid in an Eulerian frame of reference to avoid the challenges that occur in CSM.

A CFD-based model was developed for SR-FSW applications within the Ansys suite of computational software for geometry creation, meshing, and solving. The geometry is designed using Ansys Design Modeler and the Ansys Meshing utility creates an appropriate mesh. Ansys Fluent was used to discretize and solve the CFD equations using a finite volume strategy. The non-linear and model-specific equations (e.g., viscoplasticity) are implemented using custom subroutines (called “User-Defined Functions” (UDF) in Fluent). Ansys Workbench links the geometry, meshing, and solver for user friendly operation.

### 4.1 Model Domain

The simulated model geometry includes the panels to be welded, the weld tool, and any clamps or baseplates that are part of the weld fixture. An example weld geometry is shown in Figure 1. The weld

tool and clamps/baseplates are modeled as solid material while the weld panels are defined as a fluid. The model is solved in a moving reference frame centered at the weld tool and an imposed translation of the workpiece equal to the weld speed to enable steady state simulation with a fixed grid. The tool features, such as scrolls on the shoulder and threads on the pin, are incorporated by modifying the velocity boundary condition at the interface.

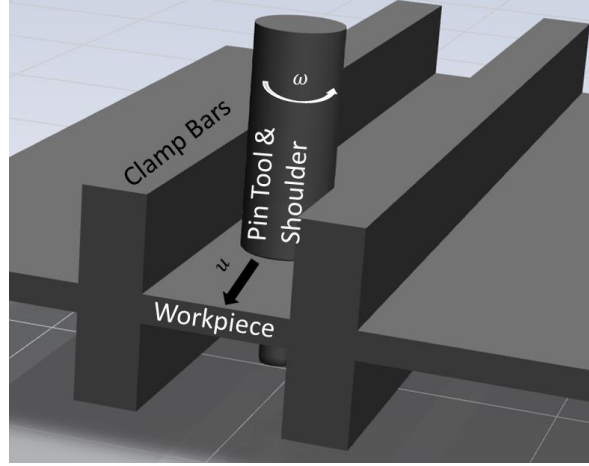


Figure 1: Schematic of the Model Domain for Self-Reacting Friction Stir Welding

## 4.2 Governing Equations

SR-FSW is a highly coupled thermo-mechanical process, and this must be considered in the development of a physics-based model. The flow and energy equations are tightly coupled: the material flow field dictates the extent of volumetric plastic heating while the temperature field affects the softening, and therefore the flow, of the workpiece material. The CFD-based simulation must solve the flow and thermal equations simultaneously, but they are presented separately here for clarity.

### 4.2.1 Flow Model

The standard continuity equation and the Navier-Stokes equations are the governing equations used in the CFD analysis to enforce mass and momentum conservation in a steady state:

$$\nabla \cdot (\rho \vec{u}) = 0 \quad (1)$$

$$\nabla \cdot (\rho \vec{u} \vec{u}) = -\nabla P + \nabla \cdot (\mu (\nabla \vec{u} + \nabla \vec{u}^T)) \quad (2)$$

where  $u$  is the material velocity,  $\rho$  is the density,  $P$  is the dynamic pressure,  $\mu$  is the effective viscosity calculated from the local strain rate and the flow stress, and  $\nabla$  is the del operator to perform vector operations in the coordinate system of interest. The flow stress is a material property that is dependent on temperature and strain rate. The modeling considerations of the flow stress is described in detail in a later section, but ultimately, the result is the effective viscosity decreases with increasing temperature and strain rate.

A constant velocity boundary condition equal to the weld speed is applied at the domain exit:

$$\vec{v}(x = x_{out}) = \vec{v}_{weld} \quad (3)$$

At the shoulder/workpiece interface, three contributions to the applied velocity are considered: (1) a default flow profile based on the flow around the pin tool ( $\vec{v}_{cyl}$ ) if the shoulder does not engage (2) tangential flow due to stick at the shoulder, and (3) inward radial flow due to the scroll pulling material toward the pin tool.

$$\vec{v} = \delta \vec{v}_{cyl} + (1 - \delta)(\vec{\omega} \times \vec{r}) - \beta_{scroll} K |\vec{\omega}| \frac{r}{|r|} \quad (4)$$

Where  $\vec{\omega}$  is the angular velocity vector,  $\vec{r}$  is the radial position vector,  $\vec{v}_{cyl}$  is the flow field around a cylinder (i.e., around the pin),  $\delta$  is the slip between the tool and workpiece,  $K$  is the scroll pitch.  $\beta_{scroll}$  is the engagement of the scroll on the workpiece and is included to account for scroll effectiveness at moving material inward due to scroll depth or other machining features. Note that the slip term,  $\delta$ , is not constant across the shoulder interface and is calculated locally as described in a later section.

At the pin tool,

$$\vec{v} = \delta \vec{v}_{cyl} + (1 - \delta_{pin})(\vec{\omega} \times \vec{r}) + ck_{pin} \vec{\omega} \quad (5)$$

Where  $k_{pin}$  is the thread pitch on the pin,  $c$  is -1 or 1 depending on the handedness of the pin treads, and the other variables are defined as above. The slip on the pin boundary,  $\delta_{pin}$ , is set to an empirical constant across the entire surface. Note the tool in SR-FSW is perpendicular to the workpiece, so the angular velocity vector  $\omega$  is parallel to the z-axis.

All free-surface boundary conditions are set to the prescribed welding speed. This is not strictly required but tends to help numerical stability and facilitates rapid convergence. Due to the high effective “viscosity” outside of the weld nugget, a zero-stress boundary condition also maintains a uniform velocity across the domain.

#### 4.2.2 Thermal Model

The heat equation for a steady-state system in terms of enthalpy is given as:

$$\nabla \cdot (\rho \vec{u} H) = \nabla \cdot (k \nabla T) + \dot{Q}_{plas} \quad (6)$$

Where  $H$  is the specific enthalpy,  $\vec{u}$  is the flow velocity vector,  $\rho$  is the local density,  $T$  is the temperature,  $k$  is the thermal conductivity, and  $\dot{Q}_{plas}$  is the plastic heating term, described in detail below. The  $\nabla \cdot (\rho \vec{u} H)$  term accounts for the convection of heat downstream relative to the tool and material flow in the nugget while  $\nabla \cdot (k \nabla T)$  represents the diffusion of heat through the domain. Frictional heating is considered on the boundary between the tool and workpiece and described below.

The rotation of the tool transports heat along the angular direction. As the tool rotational speed is fast relative to the weld speed, the temperature distribution in the tool is approximately axisymmetric, except for very near the tool/workpiece boundary. This results in net heat transfer from the tool to the workpiece on the leading edge, but a net heat transfer from the workpiece to the tool on the trailing edge.

Heat transfer also occurs between the workpiece and any clamps of the welding fixture. An empirical thermal resistance factor can be included if there is not perfect contact with the workpiece. All external boundaries consider a mixed convective and radiative heat loss to the environment:

$$Q_{loss} \left[ \frac{W}{m^2} \right] = h(T_{wall} - T_{ambient}) + \epsilon\sigma(T_{wall}^4 - T_{ambient}^4) \quad (7)$$

Where  $h$  is the convection coefficient,  $\epsilon$  is the material emissivity, and  $\sigma$  is the Stefan-Boltzmann constant. The convection coefficient is determined using engineering approximations for heat transfer from a heated flat plate in stagnant air but can be adjusted to model effects of post-weld cooling. In the case of aluminum alloys, the emissivity is quite low, and the radiative term is only a modest correction to the total heat transfer.

### 4.3 Fundamental Outputs

The Ansys Fluent CFD solver utilizes a finite volume approach to calculate the average temperature and flow characteristics (e.g., velocity and pressure) within each volume. The simulation is run in a Eulerian frame of reference on a stationary mesh. The final converged solution provides the material flow in the workpiece and the thermal profile in the workpiece, tool, and weld fixture. Temperatures at any point can be observed analogous to experimental thermocouple measurements. The flow field provides the streamlines followed by the alloy as welding occurs, as shown in Figure 2. This provides insight on mixing of the two panels and allows the material history of any point in the weld to be analyzed. This is important as the temperature and strain rate history have critical effects on the final local microstructure and ultimately on the weld strength.

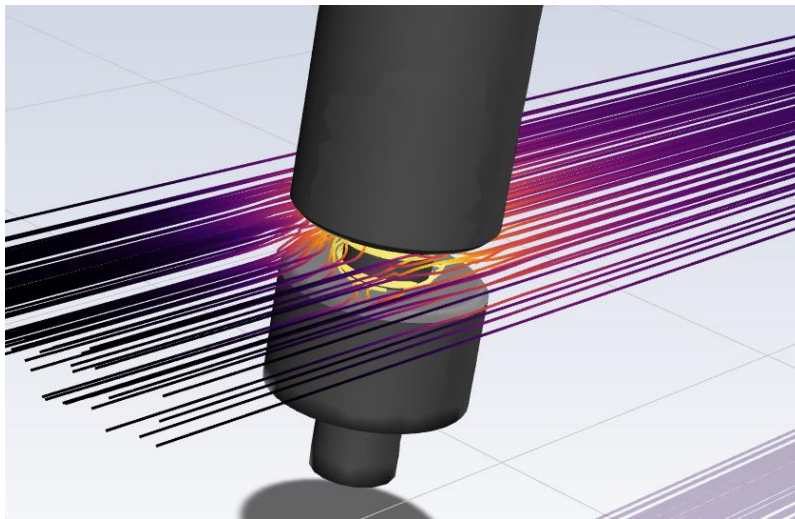


*Figure 2: Material streamlines generated using the physics-based computational model colored by temperature as it is welded.*

## 5 CFD MODEL DETAILS

### 5.1 Flow stress

The viscoplastic behavior of the metal in the SR-FSW process is modeled as an effective viscosity used in the governing flow equations. The effective viscosity,  $\mu$ , is dependent on the flow stress,  $\sigma$ , and strain rate,  $\dot{\epsilon}$ :

$$\mu = \frac{\sigma}{3\dot{\epsilon}} \quad (8)$$

The flow stress is the stress required to continually deform the material and is, in general, a function of strain, strain rate, and temperature. Furthermore, the flow stress is a material property that varies from alloy to alloy, and even from temper to temper in the same alloy. Thus, a separate constitutive model must be developed independently for any material to be included in the SR-FSW simulation. The SR-FSW process fundamentally changes the material through a combination of grain refinement and precipitate evolution. An improved model has been developed utilizing separate flow stress models for the parent material and the nugget material. If the required data is not available for the nugget material, data for a more appropriate temper can be used or the parameters can be empirically determined to best fit experimental data. The details of the implementation of this transition are given in a later section.

Several constitutive models have been developed and can be found in the literature [10, 11, 12]. The Johnson-Cook and Sheppard-Wright (aka Sellers-Taggart) constitutive models are popular constitutive models for CFD-based simulation of SR-FSW. The Johnson-Cook model considers strain hardening and tends to overestimate the flow stress at large strains and is probably most appropriate for conditions in the thermo-mechanically affected zone (TMAZ). The Sheppard-Wright model eschews the strain dependence and is appropriate when the strain hardening effects are saturated, such as occurs in the stir zone in SR-FSW [10]. Additionally, the Johnson-Cook model requires a large input data set to adequately parameterize the model across all strains, strain-rates, and temperatures of interest. For these reasons, the Sheppard-Wright model is implemented in the current physics-based model. Expanding the SR-FSW model to support other constitutive models or composite constitutive models for the flow stress is an area of future interest.

The Sheppard-Wright constitutive model is given as:

$$\sigma = \frac{1}{\alpha} \sinh^{-1} \left[ \left( \frac{Z}{A} \right)^{1/n} \right] \quad (9)$$

Where  $\alpha$ ,  $A$ , &  $n$  are material specific parameters and  $Z$  is the temperature-compensated strain rate (also referred to as the Zener-Holloman parameter):

$$Z = \dot{\epsilon} \exp \left( \frac{Q}{RT} \right) \quad (10)$$

Where  $Q$  is the activation energy related to the flow stress and another material specific parameter. The flow stress model is often parameterized using hot compression data available in the literature [13, 14, 15, 16, 17, 18] but other data, including hot torsion [19] or high pressure shear [9] tests could conceivably be used. A suggested methodology for parameterizing Equation (10) from experimental data is provided in Appendix A.

## 5.2 Friction Model

The friction between the tool and workpiece affects both the flow and thermal behavior during the welding process. The frictional force determines the flow boundary condition by affecting the extent of sticking that occurs between the tool and workpiece and generates heat when slip occurs. Thus, an appropriate friction model is necessary to ensure accurate simulation. A Coulomb friction law is used to model the applied frictional shear stress at the workpiece interface [20, 21]. The frictional stress is calculated as

$$\tau_{fric} = \mu_{FC} P_{app} \quad (11)$$

where  $P_{app}$  is the applied pressure on the shoulder (directly related to the applied pinch force) and  $\mu_{FC}$  is the Coulomb friction coefficient, which can be a function of temperature. In general, the friction coefficient decreases with increasing temperature. Furthermore, the coefficient can be convoluted by other physical phenomena, such as stick and material flow, that are known to occur in FSW process. A thin boundary layer of flowing material will result in localized plastic heating that would be difficult to distinguish from frictional heating [22].

It is important to note that a decreasing friction coefficient with increasing temperature will have a stabilizing effect on the process: a higher temperature reduces the friction, which reduces the heat generation which lowers the temperature. This can cause the behavior between welds at different operating conditions to vary less than one might naïvely expect. Furthermore, the variation in temperature across the shoulder surface has been predicted to be on the order of 100s of Kelvin and the variation in  $\mu_{FC}$  is expected to be significant. Thus, Equation (11) is applied locally at each point on the shoulder interface.

The frictional heating is calculated as a heat flux boundary condition that is a function of the relative velocity between the tool and material and the effective friction coefficient:

$$Q_{fric} \left[ \frac{W}{m^2} \right] = \mu_{FC} P_{app} \|\vec{v}_{tool} - \vec{v}_{workpiece}\| \quad (12)$$

Where  $\vec{v}_{tool}$  is the velocity of the tool face (i.e., due to tool rotation) and  $\vec{v}_{workpiece}$  is the velocity of the material at the tool interface. The relative velocity magnitude,  $\|\vec{v}_{tool} - \vec{v}_{workpiece}\|$ , is directly dependent on the extent of slip at the tool/workpiece interface,  $\delta$ .

## 5.3 Volumetric Plastic Heating

The plastic heating term is a manifestation of the viscous heating that occurs in the weld nugget:

$$Q_{plas} \left[ \frac{W}{m^3} \right] = f_{TQ} \mu \dot{\epsilon}^2 = \frac{f_{TQ} \sigma \dot{\epsilon}}{3} \quad (13)$$

Where  $f_{TQ}$  is the fraction of viscous dissipation that goes to heating (the Taylor-Quinney factor),  $\mu$  is the effective viscosity ( $\mu = \frac{\sigma}{3\dot{\epsilon}}$ ),  $\sigma$  is the flow stress of the material and  $\dot{\epsilon}$  is the strain rate. The Taylor-Quinney factor represents the fraction of input power that provides heating to the material rather than to plastic dislocations and other phenomena that represent an increase in the internal energy of the system. Often, a value of 0.8-0.9 is used [4], but in the SR-FSW process a value closer to unity is likely warranted. The high strains occurring in FSW processes lead to a situation in which the internal energy increase due to changes in crystal structure saturates and, ultimately, is small in comparison to total power input in the system. This phenomenon is observed by Lieou and Bronkhorst that shows a monotonic increase in  $f_{TQ}$  for modest strains between 0 and 0.2 [23]. The strains in the weld nugget are over two orders of magnitude larger and thus, the CFD-based model assumes a value of  $f_{TQ} = 1$  is appropriate.

#### 5.4 Stick Slip Model

The boundary condition at the tool/workpiece interface critically affects both the flow behavior and the location and magnitude of the heat generation in SR-FSW simulation. As described above, the boundary conditions at the tool-workpiece interfaces are based in part on the extent of slip and stick that occurs. The fractional slip is determined locally and can range from  $\delta = 0$  for a no-slip condition to  $\delta = 1$  to a full slip condition. A low slip condition implies that the material flows with the rotation of the tool, whereas a high slip implies the workpiece material is relatively stationary. In general, low slip/high stick results in larger weld nuggets, greater plastic heating, lower frictional heating, and greater total heat generation.

The local fractional slip on the tool shoulders is calculated by comparing the applied frictional stress to the shear yield stress and shear flow stress. The frictional stress,  $\tau_{fric}$ , is described above in Equation (11), while the shear yield stress is determined from the yield stress as

$$\tau_y = \sigma_y / \sqrt{3} \quad (14)$$

Where the temperature-dependent yield stress,  $\sigma_y$ , is determined from the literature. In this model, the local flow boundary condition at the shoulder interface should transition from a pure slip condition when  $\tau_{fric} < \tau_{yield}$  to a pure stick condition when  $\tau_{fric} > \tau_{flow}$ . For  $\tau_{yield} < \tau_{fric} < \tau_{flow}$ , a linear transition is incorporated in the model as

$$\delta(= slip) = 1 - \frac{\tau_{flow} - \tau_{fric}}{\tau_{flow} - \tau_y} \quad (15)$$

This is like the approach described by Jiang, et al [24]. This yield-based slip model has the effect of higher slip where the material is cooler, such as at front of the shoulder. Conversely, warmer material has a lower yield stress and a greater propensity to stick, although this is somewhat mitigated when using a temperature dependent friction coefficient that decreases with increasing temperatures.

Unlike at the shoulders, the slip at the pin interface is defined as an empirical constant even though it is feasible that the slip varies across the pin surface [8]. A constant slip is more numerically stable and allows for faster convergence while preliminary attempts at incorporating a pressure-dependent slip at the pin surface has resulted in divergence of the simulation.

The radial and vertical flow contributions due to the presence of the shoulder scrolls and pin threads can be defined using a slip model independent of the one utilized for the tangential boundary conditions. These flow contributions are driven by the normal force imposed at the feature surfaces and thus are related to tool engagement (i.e., how much the scrolls connect with the workpiece) rather than simple friction. This means that radial flow (for scrolls) or vertical flow (for threads) can be expected to occur even under conditions that favor slip on a smooth surface. The current model either assumes full engagement of the scrolls and threads or an equivalent slip calculated from the frictional stress. A more refined model could allow a transition to a fully engaged state depending on the applied force and material yield stress. Alternatively, incorporating a volumetric body force term to induce flow may be necessary to account for features such as scroll depth. Further analysis and development are required.

## 5.5 Thermal Parameters

Accurately modeling the heat transfer in the SR-FSW is critical to accurately predict the weld health as the temperature directly affects the flow behavior of the material and as elevated temperatures can lead to overaging of precipitate hardened alloys. The key thermal properties to consider are the thermal conductivity,  $k$ , and the specific heat capacity,  $c_p$ . In the general case, both  $k$  and  $c_p$  are functions of temperature. The crystal refinement that occurs in the weld nugget can also affect the thermal conductivity, so the SR-FSW model allows for this transition to occur during the simulation.

The thermal conductivity can vary considerably between metals, specific alloys (due to alloying elements) and even between specific tempers (due to different precipitation microstructures) [25]. For many alloys, it is possible to find room temperature conductivities in the literature or use correlations based on elemental composition [25]. Temperature dependent thermal conductivities can sometimes be found, but it is challenging, and published results may disagree [20, 26].

If possible, experimental determination of the thermal conductivity and specific heat from samples of the material to be simulated is desirable. If available, this data can be directly incorporated into the SR-FSW model and would most accurately reflect the system being welded. If direct experiments cannot be performed and relevant data cannot be found in the literature, CALPHAD (CALculation of PHase Diagrams) simulations can be performed based on the alloy composition to determine appropriate, temperature-dependent conductivity and/or the specific heat.

## 5.6 Material Transition

The SR-FSW process fundamentally transforms the material being welded due to recrystallization and precipitation effects. This manifests as different observed material properties in the weld nugget compared to the base material. In the SR-FSW model, this is implemented as a transition from using base material properties to nugget material properties. The SR-FSW model simulates this transition (base material to nugget material) using simulated maximum temperatures and maximum temperature-compensated strain rate using the following expressions:

$$f_T = \frac{1 + \tanh\left(4 \frac{T_{max} - T_{trans}}{\Delta T_{trans}}\right)}{2} \quad (16)$$

$$f_{ZH} = \frac{1 + \tanh\left(4 \frac{Z_{H,max} - Z_{H,trans}}{\Delta Z_{H,trans}}\right)}{2} \quad (17)$$

$$1 - f = (1 - f_T)(1 - f_{ZH}) \quad (18)$$

$$\phi_{composite} = f\phi_{Nugget} + (1 - f)\phi_{Parent} \quad (19)$$

Where  $f$  is the extent of transition to nugget behavior and  $\phi$  is a generic parameter of interest that undergoes significant changes between nugget and parent material.  $T_{max}$  and  $Z_{H,max}$  are the maximum temperature and the maximum temperature compensated strain rate experience by the material at the given location. The hyperbolic tangent is used to enable a smooth (continuously differentiable) transition for numerical stability.  $f_T$  is the extent of transition due to temperature effects and the transition temperature ( $T_{trans}$ ) and transition width ( $\Delta T_{trans}$ ) are semi-empirical constants related to the dissolution thermodynamics and kinetics of strengthening precipitates in precipitation hardened alloys.  $f_{ZH}$  refers to the contribution of the Zener-Holloman parameter to the transition to nugget properties. If  $f_{ZH}$  is included, the transition parameters ( $Z_{H,trans}$  &  $\Delta Z_{H,trans}$ ) are empirical constants related to the effect of recrystallization of the grains in the nugget material via the Hall-Petch relationship which may affect the macroscale behavior of the material.

This approach has been implemented for the flow stress,  $\sigma$ , thermal conductivity,  $k$ , and shear yield stress  $\tau_{yield}$  and could be applied to if data is available. It may be physically justified to separate the effects due to the temperature history and the Zener-Holloman parameter history as the precipitate evolution and grain recrystallization may have different effects on the material behavior. However, experimentally separating the effects of precipitate evolution and grain recrystallization of nugget material properties is difficult, so the combined approach in Equation (19) is appropriate without additional experiments.

## 5.7 Derived Variables

Ansys Fluent allows the user to define three additional classes of solution variables: User-Defined Memory (UDM), User-Defined Scalars (UDS), and Discrete Phase Model (DPM) variables. The UDMs allow for values to be calculated for each cell and stored for future use, such as for flow stress calculations or as additional outputs. The UDM values are not transported with the material but are calculated from the local material state. In contrast, UDS variables are transported with the material flow and can undergo diffusion and mixing. Sources and sinks can also be defined for UDS variables. DPM variables are applied to tracked particles (i.e., "Discrete Phases") that flow with the material but retain their identity.

### 5.7.1 User-Defined Memory (UDM) Variables

UDM values are calculated in each volume using User-Defined Functions (UDFs) to determine material properties or for additional outputs [27, 28]. For example, the temperature compensated strain rate (i.e., the Zener-Holloman parameter), is calculated in each cell using the cell temperature and cell strain rate:

$$Z_H = \dot{\epsilon} \exp \frac{Q}{RT} \quad (20)$$

The temperature compensated strain rate can then be utilized in other calculations, most importantly for the material flow stress and, ultimately, the effective viscosity. Other UDM values are defined to provide additional outputs that may be of interest but are not necessary for simulation. For example, torque and force calculation on the tool/workpiece interface do not affect the flow simulation but are of interest to the end user during post processing analysis.

Table 1: Example List of UDM Variables Defined in the SR-FSW Physics-Based Model

<b>UDM Variable</b>	<b>Description</b>
C_ZH_VAL, $Z_H$	Temperature compensated strain rate
C_TSTAR_VAL, $t^*$	Critical time for dissolution in the Shercliff model [29]
C_SLIP_VAL, $\delta$	Slip at the tool/workpiece interface
C_YIELD_STRESS, $\sigma_y$	Calculated temperature-dependent yield stress
C_FRICT_COEFF, $\mu_{Frict}$	Calculated temperature-dependent friction coefficient
C_FRICT_HEAT, $Q_{Frict}$	Calculated heating due to friction
C_TOTAL_FORCE_X, $F_x$	Total force in the weld direction (friction and shear stress)
C_TOTAL_FORCE_Y, $F_y$	Total force in the transverse direction (friction and shear stress)
C_TOTAL_FORCE_Z, $F_z$	Total force in the vertical direction (friction and shear stress)
C_TOTAL_TORQUE, $\tau_{total}$	Total torque (friction and shear stress)
C_VON_MISES, $\sigma_{VonMises}$	Calculated von Mises stress
C_FLOW_STRESS, $\sigma_{Flow}$	Calculated flow stress
C_TRANS_FRAC, $f$	Fraction of transition from parent material to nugget material. For use when defining effective properties

### 5.7.2 User Defined Scalar (UDS) Variables

User Defined Scalars (UDS) variables are user-defined variables that Ansys Fluent solves using the convection-diffusion equation [28]. Therefore, these variables are transported with the material flow, may undergo diffusion, and can have source and sink terms supplied by the user. In steady state, the governing equation for the  $k^{th}$  UDS variable,  $\phi_k$  is given as:

$$\frac{\partial}{\partial x_i} \left( \rho u_i \phi_k - \Gamma_k \frac{\partial \phi_k}{\partial x_i} \right) = S_k \quad (21)$$

Where  $u_i$  is the flow velocity in the  $i$ -direction,  $\rho$  is the fluid density,  $\Gamma_k$  is the diffusion coefficient, and  $S_k$  is the source (or sink) term. The UDS variables defined in the SR-FSW model do not diffuse and  $\Gamma_k = 0$ . However, numerical diffusion is a concern, and thus an appropriate meshing strategy and spatial discretization scheme is required to mitigate this effect. Meshing and discretization considerations are discussed in detail in Section 5.8.1 below.

Variables in which the current value is dependent on previous values along the flow lines are suitably modeled using the UDS approach. One-parameter precipitate evolution models can be implemented to model the fraction of strengthening precipitates. The integral of the elapsed time relative to time to full precipitate dissolution ( $\int t/t^* dt$ ) allows for the calculation of the remaining strengthening precipitates. Non-physical variables can also be recorded with a suitable choice of  $S_k$ . For example, setting  $S_k = \rho$  (due to the way the governing equation is defined, Equation (21), the material density must be included as a factor) gives the residence time.

The extent of mixing can also be explored using a UDS variable. For example, the initial panel can be specified as a simple UDS variable, with a value of 0 for the panel on the advancing side and a value of 1 on the retreating side. A hard transition is defined at the interface between panels, which can be offset from the tool centerline. The value of this variable at the weld exit shows how the welding process affects the material at the weld interface and can be used to quantify the mixing that occurs between the two panels. Unlike particle tracing methodologies, the UDS formulation allows for mixing to occur between cells. Thus, a cell can exist which consists of material from both weld panels in any proportion, which will be invaluable when considering SR-FSW of dissimilar materials.

The UDS approach can also be utilized to track the maximum value of a given variable experienced thus far by a given material volume. This is perhaps most insightful for tracking the maximum temperature experienced by the volume which is used to simulate the transition from parent material to softened nugget material. In the case of maximum temperature, the UDS variable,  $T_{max}$ , should equal room temperature ahead of the tool, increase as the tool passes, and remain constant post weld (as the workpiece cools). The source term must therefore be set so that  $T_{max}$  approaches  $T$  if  $T > T_{max}$ , but zero otherwise. The exact form of the source term is given in Table 2, but must be selected carefully. If  $S_k$  is taken as too large,  $T_{max}$  may overshoot the cell temperature, if too small it may not reach the actual maximum temperature before leaving the nugget zone. The use of a quadratic term in  $S_k$  helps achieves this and reduces oscillations by creating a smooth function.

Table 2: Example List of UDS Variables Defined in the SR-FSW Physics-Based Model

<b>UDS Variable</b>	<b>Source Term <math>S_k</math></b>	<b>Description</b>
C_MIX	0	Identifies source panel
C_SUM_TSTAR, $\int t/t^* dt$	$\rho/t^*$	Extent of precipitate dissolution
C_ZH_MAX, $Z_{H,max}$	$0 \quad Z_H < Z_{H,max}$ $10\rho(Z_H - Z_{H,max}) \quad Z_H < Z_{H,max}$	Maximum temperature compensated strain rate
C_T_MAX, $T_{max}$	$0 \quad T < T_{max}$ $100\rho(T - T_{max})^2 \quad T < T_{max}$	Maximum temperature
C_RES_TIME, $t_{res}$	$\rho$	Residence time of material through the weld
C_TOTAL_STRAIN, $\varepsilon$	$\rho\dot{\varepsilon}$	Total net strain

### 5.7.3 Discrete Phase Model

The Discrete Phase Model (DPM) in Ansys Fluent uses a Lagrangian approach to model the behavior of discrete particles as they flow through the model, in contrast to the Eulerian perspective used to solve the governing equation [30]. In the SR-FSW model, massless particles are considered and thus represent discrete material parcels of the weld material. The massless particles follow the streamlines of the material flow field. In the steady state simulation, these particles can be used to track the full material history of each material parcel after the flow and temperature profiles have been solved. The discrete particles can be injected at the weld inlet at a much higher density than the built-in “Pathlines” feature, which only creates streamlines originating from nodes on the boundary surface. Otherwise, the “Pathlines” and “DPM” particle tracks behave identically for steady state simulation, although the “Pathlines” output can also operate in reverse, which has some advantages for post processing. The DPM parcels can concentrate in certain regions of the weld outlet, whereas other regions show little or no DPM parcels reaching the weld outlet within the simulation time allowed, which could be indicative of extreme weld entrainment or, possibly, of wormhole defects.

The variables tracked in the DPM particles are analogous to the UDS variables and given in Table 2. Unlike the UDS variables, there is no mixing or exchange between the discrete particles. Thus, each particle maintains its identity and features such as weld panel origination are constant throughout the particle life. Tracking of variable maximums (i.e.  $T_{max}$  &  $Z_{H,max}$ ) is also simpler in the DPM formulation as these can be directly updated in the particle tracking subroutine, rather than relying on an ad hoc source term. It should be emphasized that the DPM relies on a one-way coupling from the flow field solution to the particle path; the state of the DPM particle does not influence the flow or temperature behavior in any way. This is convenient in that it allows for the DPM calculation to only be performed once after the flow solution has converged. However, this means that any variables which may affect the flow behavior (e.g.,  $T_{max}$  dictating the flow model to use) must be incorporated via UDS variables, not with DPM variables. Thus, the different data types available in Ansys Fluent should be seen as complementary for the SR-FSW simulation, even if the same variable is included as both DPM and UDS types.

Table 3: Example List of DPM Variables Defined in the SR-FSW Physics-Based Model

<u>DPM Variable</u>	<u>Description</u>
TP_MIX	Identifies which panel material originated from
TP_SUM_TSTAR, $\int t/t^* dt$	Extent of precipitate dissolution
TP_ZH_MAX, $Z_{H,max}$	Maximum temperature compensated strain rate
TP_T_MAX, $T_{max}$	Maximum temperature
TP_TOTAL_STRAIN, $\epsilon$	Total strain

## 5.8 Computational Considerations

The numerical model used to describe the SR-FSW is very nonlinear, and the physical phenomena are tightly coupled. Computational stability and efficiency must be considered in model development. Ansys

Fluent allows the user to adapt many aspects of the simulation, either using built-in options or based on custom user subroutines (referred to as User Defined Functions, UDFs). The solver options must be selected appropriately based on the considerations of the SR-FSW operation to improve the accuracy, stability, and computational efficiency of the simulation.

### *5.8.1 Accuracy / Meshing, Discretization, and Solver Options*

To solve the flow and temperature field, the model geometry must first be discretized into an appropriate mesh. Mesh generation is relatively simple as the geometry consists of basic geometric shapes (prisms and cylinders). Hexahedral dominant meshes are preferred over tetrahedral meshes as they are generally more numerically stable and they reduce the effect of numerical dispersion, especially when the hexahedral cells are aligned with the flow field. Fully structured meshes are used for the clamp bars and the workpiece material away from the weld, beyond about 2 or 3 tool diameters, depending on the fixture geometry. These are solid domains and only heat transfer is solved. The thermal gradients at these distances from the weld are moderate, and the heat transfer can be solved accurately with a coarse mesh. The material behavior in the weld nugget is insensitive to heat transfer occurring more than a few centimeters from the weld, further justifying the use of a coarse mesh on the far field.

The welding tool is discretized using an unstructured tetrahedral mesh to capture the curvature of the boundaries without relying on an over-refined mesh. For the region away from the tool/workpiece interface, the heat transfer is primarily in the axial direction and the higher temperature derivatives are small. As the truncation error of the 2<sup>nd</sup> order discretization is proportional to  $hT'''$ , so small high-order derivatives can allow for accurate discretization, even if the grid size is relatively large. Numerical diffusion is small relative to the thermal diffusivity so using tetrahedral cells does not introduce significant error. At the tool/workpiece interface, the mesh is conformal. That is, the faces and nodes in the workpiece body coincide with the faces and nodes on tool body. As the workpiece uses a structured hexahedral mesh, the interface faces are quadrilaterals and the first layer of cells in the tool are pyramidal and transition to tetrahedral in the bulk of the tool domain. The meshing around the cylindrical pin introduces some non-hexahedral cells and skewness, but this has not been observed to detrimentally affect the simulation.

The mesh resolution determines the accuracy of the simulation: smaller finite volumes generally increase accuracy but at increased computational costs and numerical stability. The required mesh resolution depends on the specific output(s) of interest. Global outputs, such as the integrated heat generation or average temperature, converge rapidly and can be accurately computed with a coarse mesh with cells on the order of 1mm in the nugget. Local outputs, such as temperature at a specific location or the detailed flow field, require a more refined mesh to achieve the same accuracy. Furthermore, the high gradients present in and around the weld nugget generally require smaller volumes to capture. Thus, an adaptive mesh routine refines the mesh only in regions where it would be needed. Section 5.8.3 describes the adaptive mesh routine in detail.

Several solver options must also be set to simulate the SR-FSW process, including the spatial discretization for flux calculations and the coupling between the pressure and velocity equation. These choices are summarized in Table 4. The spatial discretization can be specified for each variable solved for in the SR-FSW model. Higher order schemes are more accurate but slower (for a fixed mesh size) and generally less

numerically stable. To solve the full system of equations, Ansys Fluent separates the flow, energy, and UDS equations and solves each system sequentially in each iteration. The flow equations can be further separated into the pressure equations and the velocity equations, which can be solved sequentially or simultaneously. For the SR-FSW simulation, the coupled solver substantially improves convergence and stability because of the highly coupled and nonlinear nature of the flow.

*Table 4: Solver options for the variables considered in the SR-FSW model.*

<u>Variable</u>	<u>Option Used</u>	<u>Reason for Solver Selection</u>
Pressure and Velocity Coupling	Fully Coupled	Much improved convergence and stability, but at cost of slightly greater time per iteration compared to a sequential solver.
Momentum Spatial Discretization	1 <sup>st</sup> Order Upwind	More stable and faster than 2 <sup>nd</sup> order. No change in observed results compared to 2 <sup>nd</sup> order.
Energy Spatial Discretization	2 <sup>nd</sup> Order Upwind	Significant change in results compared to 1 <sup>st</sup> order. No observed benefit with higher order discretization.
UDS Variables Spatial Discretization	3 <sup>rd</sup> Order MUSCL	Reduced effects of numerical diffusion compared to 2 <sup>nd</sup> order.

### 5.8.2 Stability / Relaxation Factors

Numerical stability is critical to improve usability and enable multiple simulations to be performed in rapid succession. The tightly coupled nature of flow stress, flow field, temperature, shoulder stick, etc. can result in numerical challenges, especially at the beginning of the simulation, or if changes are made to the mesh. If these issues are not considered, the SR-FSW simulation may fail to converge. Simulation failures require manual intervention to continue or exit the program. If several simulations are scripted to be run sequentially, this can result in several hours or days of lost simulation time. Thus, a highly robust simulation strategy can greatly improve performance and increase simulation throughput by facilitating automatic sequential simulation of designated test cases without manual intervention. Several areas of the simulation have been identified as being potentially unstable, and mitigation strategies have been developed to balance the need for robust simulation and computational accuracy.

The SR-FSW model is solved using an iterative process. Consider a solution estimate consisting of an initial estimate for the value of all variables in each cell. The error vector of the solution estimate is given in terms of the true solution:

$$\epsilon = \phi - \hat{\phi}_i \quad (22)$$

Where  $\phi$  is the true solution and  $\hat{\phi}_i$  is the solution estimate at iteration  $i$ . Unfortunately, the true solution cannot be known – if it were known, this iterative process would not be necessary. Instead, the solver aims to find  $\hat{\phi}_i$  such that the linearized form of the governing equations is satisfied:

$$\mathbf{A}\hat{\boldsymbol{\phi}}_i + \mathbf{b} = \mathbf{0} \quad (23)$$

Where  $\mathbf{A}$  is the coefficient matrix representing the discretized governing equation and  $\mathbf{b}$  is a constant vector incorporating the source terms. At each iteration, governing equations are linearized around the current solution estimate to determine  $\mathbf{A}$ , the residual of Equation (23) is calculated, and the variable updates,  $\Delta\hat{\boldsymbol{\phi}}$  is determined. The solution estimate can be updated using:

$$\hat{\boldsymbol{\phi}}_{i+1} = \hat{\boldsymbol{\phi}}_i + \Delta\hat{\boldsymbol{\phi}} \quad (24)$$

In a well-behaved and stable problem, the equation residuals and variable updates should decrease which each iteration. However, numerical stability is especially a concern in highly coupled systems, such as the SR-FSW model. Large variable updates can cause the solution estimate to overshoot and result in an updated solution estimate that is worse than the original estimate. This can be mitigated using relaxation terms to reduce the size of the step taken in each iteration:

$$\hat{\boldsymbol{\phi}}_{i+1} = \hat{\boldsymbol{\phi}}_i + \alpha\Delta\hat{\boldsymbol{\phi}} \quad (25)$$

Where  $\alpha$  is the relaxation factor in the range  $0 < \alpha \leq 1$ . In general, larger values of  $\alpha$  accelerate simulations, but reduce stability. Furthermore, the relaxation approach can be applied to both variables (e.g., temperature) and derived material parameters (e.g., viscosity). There is no requirement that the relaxation factor  $\alpha$  be the same for all variables, nor is it required to be constant for the entirety of the simulation. Thus, the relaxation factor can be adapted during the simulation run in response to the observed simulation behavior: a conservative approach can be taken when the simulation shows signs of instability while a more aggressive approach can be taken when the simulation has stabilized.

#### Flow Stress and Plastic Heating

The effective viscosity is a strong function of temperature and the volumetric heat generation is a strong function of effective viscosity. This tight coupling can result in significant computational challenges to the simulation stability and efficiency. The simulation begins at room temperature with applied velocity boundary conditions on the pin surface. At room temperature, any applied strain will result in substantial plastic heating. If care is not taken, a rapid temperature rise will occur after the first solution iteration. This will cause the flow stress to drop dramatically on the next iteration, resulting in very little heat generation. At best, this will cause the solution to oscillate with each iteration and each iteration will be slowed by the need for Fluent to maintain stability by using more expensive matrix preconditioners. Most likely, this scenario will cause the solution to diverge within a few dozen iterations.

Several features have been incorporated to mitigate this instability. (1) During the first two iterations, the effective viscosity is artificially reduced (and constant) to allow for an approximate flow field to develop. (2) During these initialization iterations, the volumetric heating is zero and then slowly ramps up to the full plastic heating prediction over ten iterations. (3) A relaxation term is included in the viscosity update calculation to mitigate the effects of any large changes in the viscosity. This is important because the viscosity can span several orders of magnitude in the final solution. (1) & (2) are only applied for a limited number of iterations, but (3) is included throughout the simulation. These stability improvements do come at a slight cost of increased computation, but the effect is small. The initialization of the viscosity and volumetric heating occurs over the first ten iterations and can be completed on a coarse grid. The viscosity

relaxation term is set so that the simulated viscosity will be within 99.99% of the final value within six iterations. Given that convergence usually takes on the order of 100 to 1000 iterations, and that improved stability generally improves the condition of the underlying matrix, this is a tradeoff well worth making.

#### Stick/Slip Transition

The relationship between extent of slip at the shoulder interface and the temperature is perhaps a more challenging issue regarding stability. Recall that the extent of slip depends on the shear yield stress of the workpiece material which is a function of temperature. That is, as the material heats up, the yield stress decreases and there is a greater propensity of the material to stick and flow with the tool shoulder. However, greater flow results in greater plastic heating and higher temperatures. This can result in positive feedback loop that creates a rapid temperature rise, overshooting the converged, stable solution and ultimately diverging leading to solution failure. This is especially problematic if the slip/stick model had a sharp delineation between the slip regime and stick regime but remains a challenge even with a broad transition from slip to stick.

To improve the stability of the stick/slip model, a relaxation term has been included to avoid the conditions that create a positive feedback and lead to divergence.

$$\delta_{slip} = \delta_{old} + \alpha(\delta_{new} - \delta_{old}) \quad (26)$$

During the initialization phase,  $\alpha$  is set to a value 0.15, which is rather conservative, to maintain stability. Unlike the viscosity and heat generation initialization, the number of iterations is not fixed. Rather, the slow update to slip is maintained until the global average slip value stabilizes, at which point  $\alpha$  is increased to 0.5 to speed convergence. This is achieved using Fluent's "ON\_DEMAND" UDF macro functionality. For stability reasons, the more conservative  $\alpha = 0.15$  value is used any time changes are made mid-simulation, including changes in grid refinement, physical parameters, or operating conditions. The Scheme script file read by Ansys Fluent tracks the change in slip every few iterations. When the total average slip changes by less than a specified threshold in each iteration, the simulation will switch to using a higher relaxation factor for the slip model to speed up the simulation as it approaches the final converged state.

#### Setting Fluent Solver Relaxation Factors

Ansys Fluent allows the user to set a relaxation factor for each of the scalar variables being solved for [27, 30]. In the case of momentum and pressure, these are explicit factors applied to the variable update performed during each solver iteration as described above:

$$\phi = \phi_{old} + \alpha\Delta\phi \quad (27)$$

For the other variables, the relaxation is applied implicitly to the discretized equations [30]:

$$\frac{a_p\phi}{\alpha} = \sum a_{nb}\phi_{nb} + b + \frac{1-\alpha}{\alpha}a_p\phi_{old} \quad (28)$$

Where the subscript  $nb$  refers to neighboring cells and  $a$  and  $b$  are coefficients arising from the spatial discretization and source terms, with  $a_p$  referring to the diagonal elements and  $a_{nb}$  referring to the off-diagonal elements. A lower value of  $\alpha$  increases the condition number of the matrix by making it more

diagonally dominant. This improves the computational stability but slows the rate of convergence. However, since solving well-conditioned linear systems can often be done faster than ill-conditioned ones, the net effect on the computational time may be faster with a smaller relaxation factor.

In general, during the initial phase of simulation, the model is less stable and more ill-conditioned due to the rapidly changing flow and thermal states and the coupling with physical parameters, especially the flow stress, and the stick vs. slip boundary condition. For this reason, the relaxation factors are initially set to be conservative but allowed to increase as the solution stabilizes to accelerate convergence. This strategy is applied to the momentum and pressure explicit relaxation terms, implicit relaxation for the  $T_{max}$  and  $Z_{H,max}$  UDS equations and implicit relaxation of the energy equation. For the energy equation, a distinct numerical noise filter feature is turned on (using the command “/solve/set/advanced/energy-numerical-noise-filter”), otherwise  $\alpha = 1.0$  is unstable.

### 5.8.3 Mesh Adaptation

Another approach to speed up the simulation is to adapt the mesh during the simulation run. The SR-FSW model is initially solved on a coarse mesh that can be solved quickly and robustly. This provides a better starting point for a more refined mesh to be used for the final analysis. Several refinement strategies have been developed to address different needs of the simulation.

The tool/workpiece interface is an area of the model domain where many physical phenomena of interest occur. The modeled slip can vary considerably across the shoulder surface due to the significant temperature variations. There is also a boundary layer in the flow at the tool/workpiece interface. Increasing the mesh refinement at the interface increases the accuracy of the simulation overall and may be the most important area to have a refined mesh, and this is considered in the Scheme script used to drive the simulations. Areas of high strain rate in the weld nugget are also prioritized to better capture the weld nugget shape and to capture the high thermal and momentum gradients.

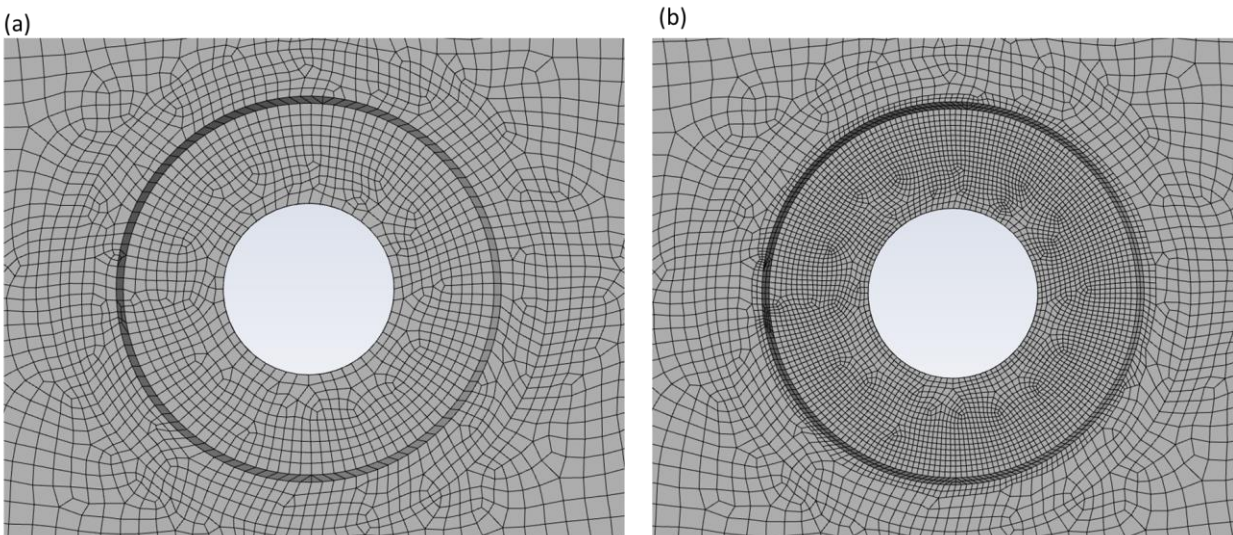


Figure 3: (a) Initial mesh near the tool/workpiece interface. (b) Mesh after one level of refinement near the pin tool.

The advantage of adaptive meshing is two-fold. First off, fewer iterations are required on the refined grid when using solutions from the coarse grid as the initial state. Secondly, the grid refinement can be limited to regions where an improvement in accuracy is needed. For the SR-FSW model, most of the features of interest are in the immediate vicinity of the weld nugget. The heat transfer that occurs post weld and through the sides does not require a refined mesh to accurately capture the temperature and flow profile. However, once the simulation has converged in the nugget, refinement of the surrounding workpiece is performed to facilitate more detailed post processing analysis. This is necessary to observe the final simulated weld cross sections in detail but only requires a few additional iterations to converge.

However, mesh refinement during simulation must be done carefully to ensure stability. When the mesh is refined during simulation, the values of the scalars are passed from the parent cells to the refined child cells. However, the UDM variables are not updated until the end of the first iteration. In particular, the viscosity (which is highly sensitive to temperature and strain rate) is incorrect in the child cells, potentially leading to simulation failure. Additionally, the propagation of the results from a coarse grid to a refined grid can result in unreasonably large gradients being calculated for the first few iterations. Thus, some of the relaxation features described above are also incorporated when restarting a simulation after a mesh update to smooth the transition, although not to the same extent as with starting the simulation.

## 6 CALCULATED SIMULATION OUTPUTS

Postprocessing of the temperature and flow data generated from a SR-FSW simulation provide derived outputs that may be of interest and are instrumental in determining weld health. These outputs can be used for additional validation as direct temperature measurements are limited and direct flow observations are minimal. These outputs can be used to analyze the mixing effectiveness in the weld and characterize the effect of weld offsets. The behavior at the tool interface can be explored, and the total time vs. temperature history can be analyzed and correlated to weld health. In some cases, these can simulate physical experiments for validation, but the computational analysis provides the ability to perform experiments which cannot be performed physically or at much lower cost.

### 6.1 Tracers

Tracer studies are occasionally used to explore the behavior of the material flow during the welding process. Small beads or strips of dissimilar material are inserted into the workpiece prior to the weld. The dissimilar material is selected to enable high contrast from the base material during the post weld x-ray analysis. This allows visualization of the material transport that occurs in the welding process.

The CFD-based SR-FSW can perform numerical experiments analogous to tracer studies by tracking the flow streamlines from the weld entrance to the weld exit. The simulation approach offers two key advantages over the physical experiments: (1) the numerical “tracers” do not affect the flow behavior, which may occur with the inclusion of physical tracers, and (2) numerical “tracers” can be inserted in any orientation and at any position. It is possible to perform numerical tracer studies on planes oriented in all three orthogonal directions simultaneously in a single simulation.

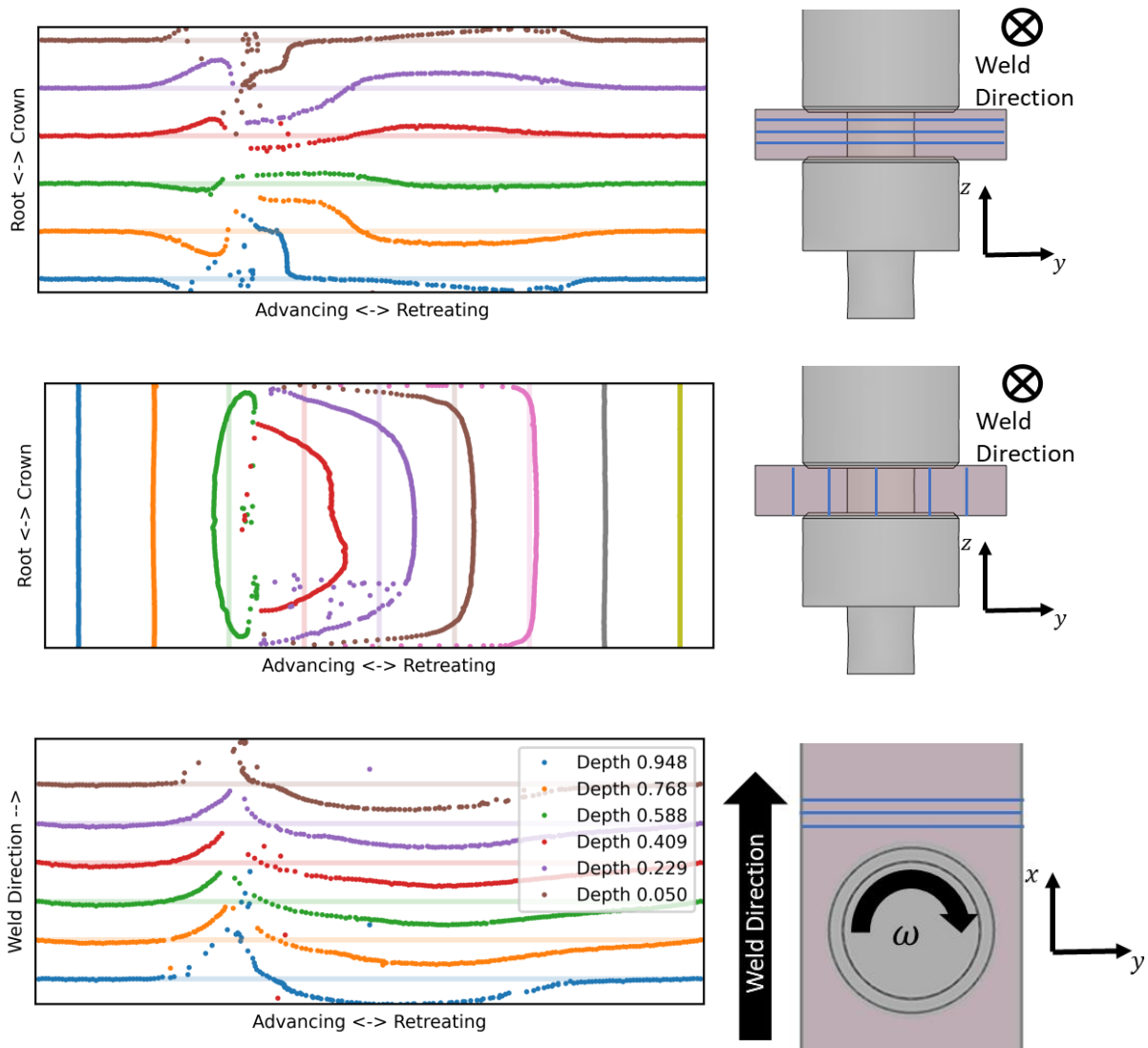
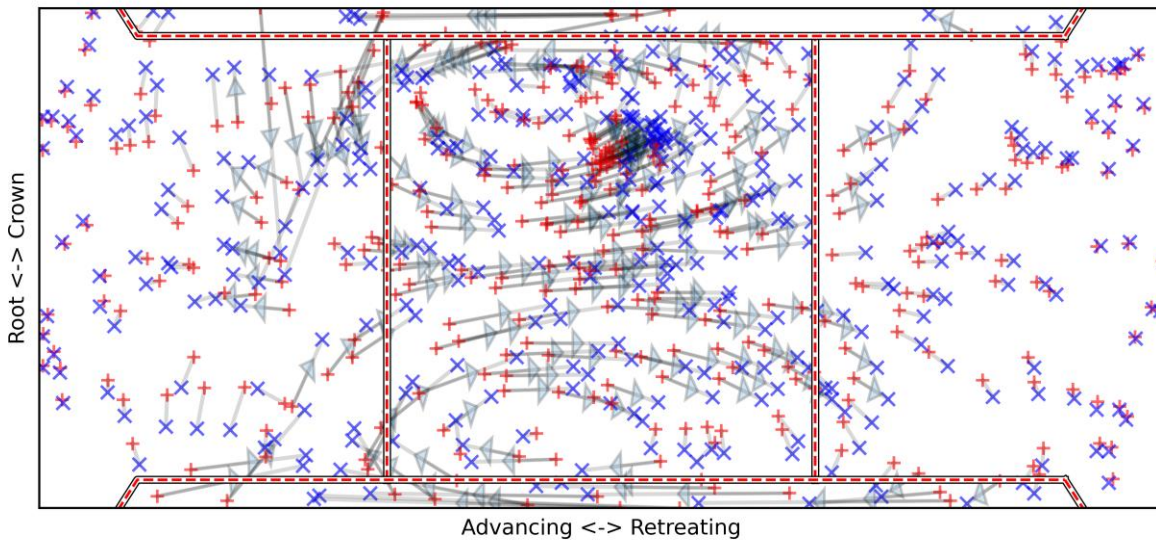


Figure 4: Numerical tracer studies of planes orientated parallel to the weld surface (a), parallel to the weld seam (b), and parallel to the transverse plane (c). The blue lines on the tool schematic indicate the initial orientation of the tracer material. For (a) and (b) the view is orientated in the direction of the weld. For (c), the view is from the top and the various tracers show results at different depths from the crown surface.

Figure 4 shows example numerical tracer studies with tracers inserted as planes along the three orthogonal orientations. The light lines in the plots show in initial location of the tracers while the dark points represent the final location after welding. Several planes are shown at each orientation as indicated by the blue lines on the SR-FSW tool schematic. Note that the steady state simulation eliminates the simulation variability in the weld direction, so Figure 4(a) and Figure 4(b) represent the simulated tracers across the full weld length. This analysis can provide increased understanding of the flow field and can be compared to experiments for validation and calibration. Understanding how material is transported during the welding process can support the development of novel tool designs that aim to affect the nugget flow field to enhance material mixing.

Unlike physical tracer studies, numerical tracer studies can insert a randomly scattered population of tracers and relate the initial location to the final location. This can provide a clearer view of the overall material transport by showing material recirculation or entrainment that occurs in the weld nugget. Figure 5 shows the initial and final locations of tracers randomly scattered across the domain. Although the arrows provide an indication of net material transfer, the full path is considerably more complicated. For example, material on the advancing side can flow around the full circumference of the pin tool and ultimately end up very close to the initial point.



*Figure 5: Scattered tracer experiment showing how material is transported transverse to the weld direction. The tracers' origin locations (Red +) and final locations (Blue x) are indicated. The figure orientation is such that the weld is progressing into the page.*

## 6.2 Mixing Maps

The extent of mixing and bonding between the two panels can be reported by labeling the weld inlet material based on the location. In the simplest application with the weld tool centered between the panels, the workpiece at location  $y < 0$  is marked as being from one panel, while the rest is marked as being from the other panel. Weld offsets can be simulated by setting the transition point at a value other than zero. This can provide insight on the extent of bonding and ultimately will be required for the simulation of welding of dissimilar materials.

The mixing analysis can be performed using DPM (Lagrangian) variables or UDS (Eulerian) variables. In the Lagrangian approach, the material parcel is considered as a point massless particle that travels along the streamlines. The DPM point maintains its panel identity throughout the simulation and the data provided at the outlet is a cross section of material consisting of points which are either from the advancing side panel or the retreating side panel, but not points which are a mixture of both. In contrast, the Eulerian approach solves to the fraction of material from each panel that is present in each finite volume. Mixing of the weld panel material can and does occur at the microscale and the material at the weld outlet may have originated from either panel in varying proportion.

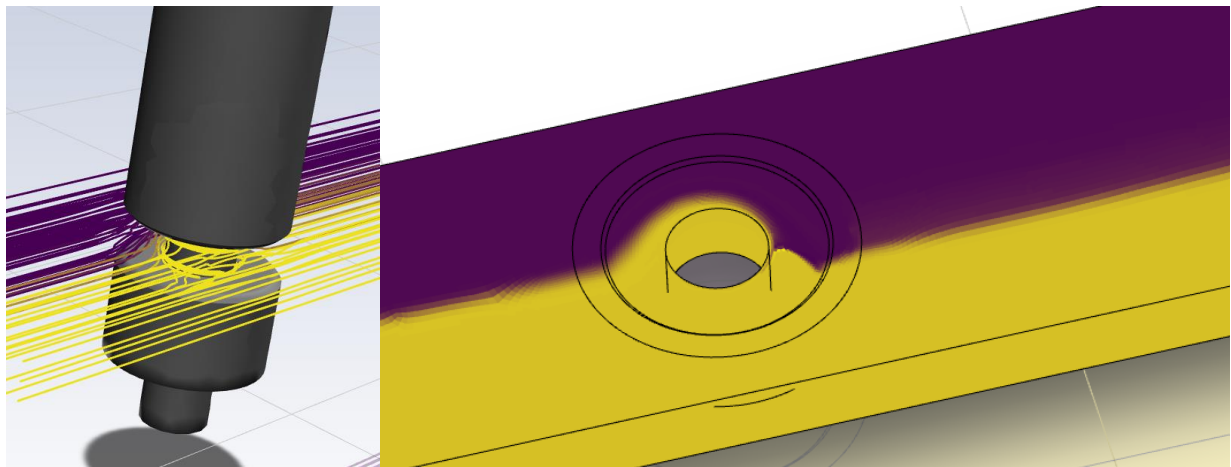


Figure 6: Streamlines colored by initial material (Left). Contours on weld seam surface colored by initial material (Right).

Example cross sections showing the origin panel contributions using the DPM and UDS results from the same simulation are shown in Figure 7. Both approaches are qualitatively similar, but the interface is considerably softer when using the UDS result due to the microscale mixing that occurs.

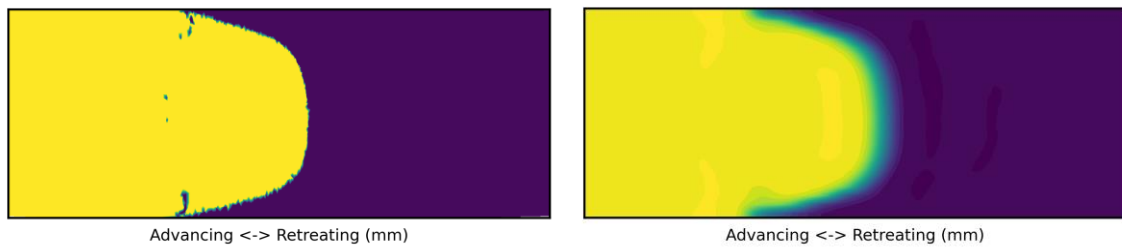


Figure 7: Weld cross section showing origin panel of material using the DPM/Lagrangian (Left) and UDS/Eularian (Right) analysis.

Figure 7 shows results for a centered weld for demonstration purposes, although offsets and inserted shims can be studied as well, as is done in Figure 8. Analysis of the origin of the material in the weld nugget can provide insight on the effectiveness of mixing, can be used to analyze the effects of changing pin tool designs, and can be used as another datapoint of comparison for experimental validation. This approach also provides a framework for simulating dissimilar welds in which the material on the advancing side is different from the retreating side. The physical properties can conceivably be modified *in silico* in response to changing local material fraction.

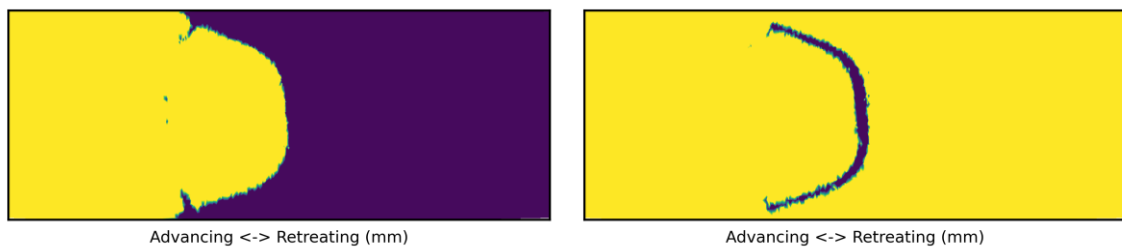


Figure 8: Weld cross section showing origin panel of material with a welding offset (Left) and showing final material transport of an inserted shim between the workpiece panels (Right).

### 6.3 Cross sections

By tracing the material streamlines, it is possible to create contour plots of the weld cross section to visualize the history of the material during the SR-FSW process. These contour plots are created by analyzing the streamlines which terminate at each point in the cross section. For each contour plot, hundreds or thousands of streamlines are analyzed to provide adequate density of data to resolve the features of interest, mostly those related to the weld nugget.

Each streamline can be represented as a series of data points containing space  $(x, y, z)$  and time data as well as the simulated data available at that point. Any combination of the dependent variables can be analyzed, which could include those directly solved for such as temperature, or derived values such as the Zener-Holloman temperature-compensated strain rate.

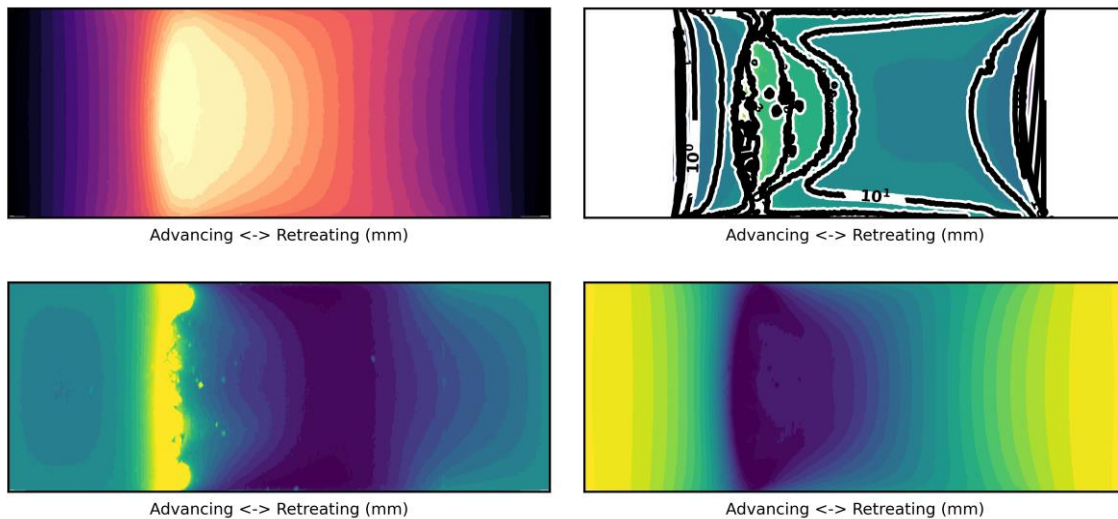


Figure 9: Example contour plots obtained by tracing streamlines to weld exit and colored by: maximum temperature (Top Left), maximum strain rate (Top Right), material residence time (Bottom Left), and simulated Vickers' hardness using the model by Shercliff et al. [29] (Bottom Right).

Each streamline may contain hundreds or thousands of data points to distill to a single value to represent a single point in the weld cross section using a mathematical formulation to obtain a value of interest. For example, the maximum temperature is obtained by simply finding the maximum temperature that occurs along the streamline – all other data is ignored. The total strain is the result of integrating the strain rate magnitude along the streamline path. Some of the potential outputs are given in Table 5.

Table 5: Output variables and the mathematical operation applied to each streamline.

Output Variable	Mathematical Operation Applied to Each Streamline
Maximum temperature	$\max T$

Maximum strain rate	$\max \dot{\epsilon} $
Total Strain	$\oint  \dot{\epsilon}  dt$
Residence Time	$\oint dt$
Time at Temperature greater than $T_{ref}$	$\oint dt$ when $T > T_{Ref}$
Maximum Zener-Holloman Parameter	$\max Z_H = \max \dot{\epsilon} \exp \frac{Q}{RT}$ , when $T > T_{ZH,cutoff}$
Modeled Grain Size (Hall-Petch)	$\ln d = a - b \ln Z_{h,max}$
Remaining Precipitate Fraction [29]	$1.0 - g \left( \oint \frac{1}{t^*} dt \right)$
Precipitate Size Distribution [31, 32]	$n(R, t) = \oint r(R, T) dt$

If a suitable model is available, more complex physics can be captured by integrating over the streamlines. The evolution of hardening precipitates can be simulated using a simplified dissolution model [29] or using a more complicated population balance model [31, 32]. The concentration and size of the resulting precipitates (and remaining solute to provide solution strengthening) directly affect the cross-sectional weld hardness and the tensile strength.

#### 6.4 Shoulder Interface

The CFD-based numerical model has the potential to provide insight on behavior occurring at locations which are difficult to directly observe such as at the tool/workpiece interface. The tool/workpiece interface is a region of significant interest as the shoulders drive much of the flow and heat generation which strongly affects the material softening and weld nugget shape. This can have a significant impact on the strength of the final weld.

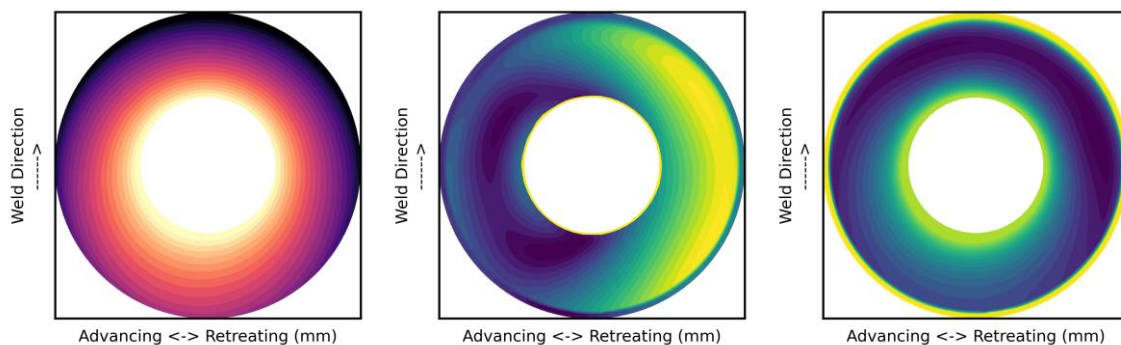


Figure 10: Example results at the crown/workpiece interface showing the (a) temperature, (b) material velocity, and (c) local slip.

Any of the available variables can be analyzed at the tool/workpiece interface, although determining useful correlations to predict weld health requires further analysis and research. A weld which has high temperature variability across the weld interface may have different performance characteristics than one which is more uniform, even if the average temperature is the same.

The friction and local slip are temperature dependent and determine the degree of tool engagement. This defines the flow velocity boundary conditions. Depending on the friction model used and the stick-slip model used, the relationship between the local tool velocity and temperature can be non-monotonic. An increase in temperature typically reduces the friction coefficient, encouraging slipping. However, the material is softer at higher temperatures, reducing slippage.

Understanding the material behavior at the shoulder/workpiece interface is important for assessing the tool effectiveness and could support the development of novel tool designs. The physics-based numerical model can output physical details at the shoulder/workpiece interface, including temperature, applied flow velocity, extent of slip, etc., as shown in the example in Figure 10. Analyzing this data could help explore novel tool designs by quantifying the expected changes in material behavior. Exploration of the stick/slip behavior may lead to insight on future tool design to better understand and mitigate the tradeoffs occurring in the SR-FSW process. High temperatures can lead to overaging and weak welds, but low temperatures can result in limited bonding between the panels. Changes in the shoulder scrolls may affect the effective friction coefficient and flow, leading to better (or worse) mixing of material. The magnitude of these changes on the temperature and flow profiles could be determined from the numerical model and could provide insight on the suitability of the proposed changes as changes in the temperature profile and weld nugget shape will affect the local material strength.

## 6.5 Output Parameters

Compared to physical experiments, numerical simulations can explore the potential operational parameter space more expansively, quickly, and cheaply and without risk of tool damage or wear. Single-valued output parameters can be used to compare the results from different simulations. Some output parameters, such as total input power and temperature at specific locations, can be compared directly to experiment and used as validation if appropriate experimental data is available. The variation of output parameters with respect to changing in input operational parameters can be visualized using a contour plot, as shown in Figure 11 for the average temperature at the tool/workpiece interface.

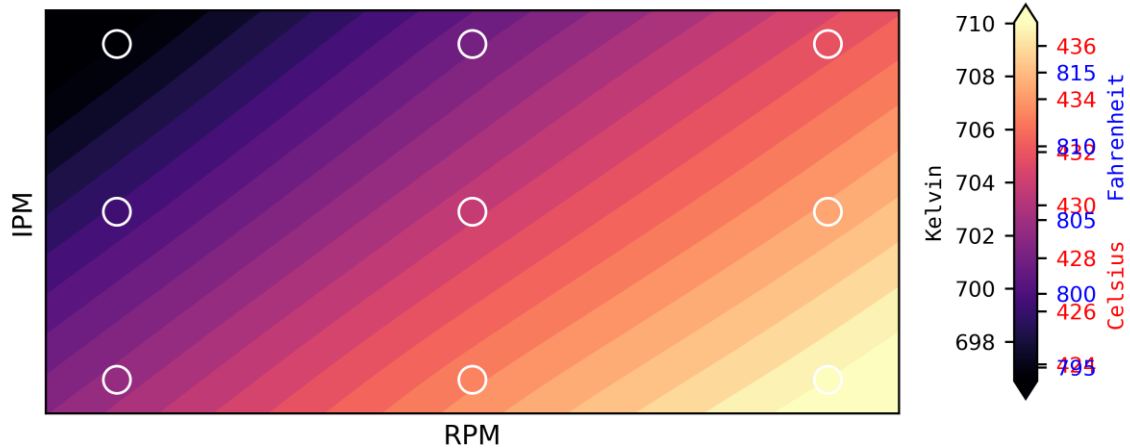


Figure 11: Simulated average temperature at tool interface as a function of operational parameters (RPM and IPM).

The simulated output parameters could be compared to measured features of interest to identify empirical correlations between operational conditions and weld health. Such correlations are valuable for extending the predictability of the model to quantify behavior that is not directly simulated, such as tensile stress or weld defects.

Table 6: Example output parameters from SR-FSW simulations.

Output Parameter	Description
max-temp-op	Maximum temperature in the entire domain
tool-avg-temp-op	Average temperature at the tool/workpiece interface
surf-avg-temp-op	Average temperature on the surface of the welded material
out-avg-temp-op	Average temperature of the weld material as it exits the domain
shoulder-frict-op	Average friction coefficient on the crown and root shoulders
avg-slip-op	Average slip on the crown and root shoulders
total_heating	Total heating generated in the welding process
energy_per_meter	Total heating generated per length of weld
total-plastic-heat-op	Total heating due to plastic generation
total-fric-heat-op	Total heating due to friction

## 7 CONCLUSIONS

The SR-FSW model presented here uses fundamental CFD-based concepts with a viscoplastic model of the flow stress to simulate the material flow during welding. Plastic deformation and friction generate heat

and heat transfer is simulated throughout the domain. Ultimately, the material flow characteristics and temperature profile are calculated at each point in the welding region including the weld nugget. From this simulated data set, numerous variables of interest can be calculated, including strain rate and temperature history at each point post weld. These histories directly influence the resulting microstructure and the weld strength.

The model is highly extensible and can be generalized to various alloys, provided appropriate physical parameters can be obtained or estimated, although fully parameterizing the model can be a challenge. The availability of physical parameters in the literature is very alloy dependent, but engineering approximations can often be made. The flow stress in the physics-based model generally comes from hot compression data, which do not achieve the extreme strains and strain rates occurring in SR-FSW. High pressure shear stress experiments aim to develop constitutive models under conditions more like those experienced in SR-FSW, but have challenges related to accurately measuring the effective shear rate and being unable to separate strain-rate and temperature [9, 33]. Other parameters, such as friction or slip coefficients, are empirical and may need to be adjusted for each system to best fit the available data.

Despite these challenges, physics-based modeling of SR-FSW can provide significant cost savings and performance improvements when developing a new SR-FSW process, testing novel tool designs, or creating advanced control algorithms. Truly novel tool designs and broad process windows can be tested in a simulated environment at low cost and without the risk of tool damage. The limited availability of tooling alloys can limit the number of distinct tool designs that could be tested, so judicious selection of candidate designs is prudent. Furthermore, ideal operational conditions depend on the tool design and better performance can be achieved by optimizing both operational conditions and tool design simultaneously than individually. Designs that have a low probability of success can be avoided, providing significant cost savings in tool manufacture and testing. Designs that would not have been studied using traditional approaches may prove promising and worthy of further investigation.

## 8 APPENDIX: FLOW STRESS PARAMETERIZATION

The Sheppard-Wright constitutive model is given as:

$$\sigma = \frac{1}{\alpha} \sinh^{-1} \left[ \left( \frac{Z}{A} \right)^{1/n} \right] \quad (29)$$

Where  $\alpha$ ,  $A$ , &  $n$  are material specific parameters and  $Z$  is the temperature-compensated strain rate (also referred to as the Zener-Holloman parameter):

$$Z = \dot{\epsilon} \exp \left( \frac{Q}{RT} \right) \quad (30)$$

Where  $Q$  is the activation energy related to the flow stress.

Combining Equation (29) and (30) and rearranging gives:

$$\dot{\epsilon} = A (\sinh \alpha \sigma)^n \exp \left( -\frac{Q}{RT} \right) \quad (31)$$

To fully characterize the Sheppard-Wright model, the four parameters ( $\alpha$ ,  $A$ ,  $n$ , &  $Q$ ) can be found using experimental hot compression data ( $\sigma$  vs.  $\dot{\epsilon}$  vs.  $T$ ) performed on the material of interest. Historically, the parameters were determined by performing linear regression on plots of  $\sigma$  vs.  $\ln \dot{\epsilon}$  and  $\ln \sigma$  vs.  $\ln \dot{\epsilon}$  on experiments performed at constant temperature [13, 16, 14, 15]. For small  $\alpha \sigma$  (generally taken as  $\alpha \sigma < 0.8$ ),  $\sinh \alpha \sigma \approx \alpha \sigma$  and the plot of  $\ln \sigma$  vs.  $\ln \dot{\epsilon}$  is linear. For large  $\alpha \sigma$  (generally taken as  $\alpha \sigma > 1.2$ ),  $\sinh \alpha \sigma \approx \frac{\exp \alpha \sigma}{2}$  and the plot of  $\sigma$  vs.  $\ln \dot{\epsilon}$  is linear. Using the slopes and intercepts of the linear regressions, values for  $\alpha$  and  $n$  can be computed individually for each temperature. The mean values are then taken as the true values. Linear regression between  $1/T$  and  $\ln[\sinh(\alpha \sigma)]$  can be used to determine a value of the activation energy  $Q$  for each strain rate tested. Again, a mean value is used as the “true” value of the Sheppard-Wright activation energy. Plotting  $\ln[Z]$  vs.  $\ln[\sinh(\alpha \sigma)]$  is used to determine  $A$  and  $n$ . Note that a value of  $n$  had been determined from the plots of  $\sigma$  vs.  $\ln \dot{\epsilon}$ . Although the derivation suggests that these values should be the same, they often are not, and this is often conveniently ignored in the literature [13].

Relying on a series of linear regressions to parameterize the Sheppard-Wright is simple but inaccurate and is not necessary with modern computing capabilities. The parameterization relies on the approximations that  $\sinh \alpha \sigma \approx \alpha \sigma$  or  $\sinh \alpha \sigma \approx \exp \alpha \sigma$  to perform the linear regression analysis. At best, this requires a preliminary estimate of  $\alpha$  and an acceptance of a truncation error of up to 10% (if the conventional cutoffs of 0.8 and 1.2 are used for  $\alpha \sigma$ ). Some literature analyses (e.g. [13]) do not seem to segregate the data into high and low stress regimes and perform  $\sigma$  vs.  $\ln \dot{\epsilon}$  regression and  $\ln \sigma$  vs.  $\ln \dot{\epsilon}$  on all the available data, which, strictly speaking, is not valid.

This analytical approach also effectively requires the hot compression experiments to be performed on a dense grid of strain rate and temperature values since the regressions are performed on experiments at

constant temperature or constant strain rate. If both temperature and strain rate vary, this analysis cannot be used. Furthermore, justification is not provided when using an average of values obtained through independent linear regressions and this is not expected to provide the best fit to the combined data set.

For these reasons, performing a simultaneous analysis is preferred. Tello et al. [17] estimated the Sheppard-Wright parameters for AA2219-T87 simultaneously using nonlinear optimization techniques to minimize the error between the model predicted stress and measured stress. This offers two key advantages: (1) the full data set is utilized for parameter estimation and (2) the truncation error due to linearization of the hyperbolic sine factor is avoided. However, this approach has limitations. Even on modern computers, estimating four nonlinear parameters can be computationally expensive and there is no guarantee of finding a global minimum. Indeed, Tello et al. relies on a local search method to estimate their parameters [17].

However, an alternative linearization and optimization approach could utilize advantages of both methods. By limiting the number of parameters to be considered in the global search, the estimation can be performed efficiently and with good confidence that a global solution can be found. Recall the Sellers-Taggart relationship between strain rate, stress, and temperature.

$$\dot{\epsilon} = A(\sinh \alpha\sigma)^n \exp\left(-\frac{Q}{RT}\right) \quad (32)$$

Taking the natural logarithm of both sides and rearranging gives.

$$\ln \dot{\epsilon} + \frac{Q}{RT} = n \ln(\sinh \alpha\sigma) + \ln A \quad (33)$$

Where  $\ln \dot{\epsilon} + \frac{Q}{RT}$  is equivalent to the logarithm of the temperature compensated strain rate,  $\ln Z_H$

$$\ln Z_H = n \ln(\sinh \alpha\sigma) + \ln A \quad (34)$$

Performing a linear regression on  $\ln Z_H$  vs.  $\sinh \alpha\sigma$  allows for determination of the stress exponent,  $n$ , and  $\ln A$ , as well as the coefficient of linear regression,  $R^2$ . This will provide the best fit values of  $n$  and  $\ln A$  for given values of  $Q$  and  $\alpha$ . A global search can then be performed on  $Q$  and  $\alpha$  to maximize  $R^2$ . This allows the optimization routine to operate only on two parameters, providing much stronger confidence that a true global optimum can be found in a short time.

The linear regression minimizes the sum squared errors of  $\ln Z_H$ . Maximizing  $R^2$  ensures that any scaling effects due to the  $\frac{Q}{RT}$  term do not affect the optimization search as a direct minimization of the sum of squared errors would do. If the sum of squared errors is minimized directly the solution may converge to a smaller  $Q$  as that results in smaller values of  $\ln Z_H$  and therefore, smaller absolute values of the errors, in general, even though the relative error is larger.

This approach is equivalent to minimizing the error of  $\ln(\sinh \alpha\sigma)$ , and approximately equivalent to using the error of the logarithm of the stress at low stresses, and the direct error of the stress at high stress, which ensures both high and low stress states contribute meaningfully to the final regression.

## 9 REFERENCES

- [1] W. M. Thomas, E. D. Nicholas, J. C. Needham, M. G. Murch, P. Temple-Smith and C. J. Dawes, "Friction Stir Butt Welding, International Patent Application No. PCT/GB92," *GB Patent Application No.9125978.8*, 12 1991.
- [2] A. C. Nunes, "Understanding Friction Stir Welding," *NASA*, Vols. NASA/TM-2018-219854, 2018.
- [3] G. Bjorkman, M. Cantrell and R. Carter, "Self-Reacting Friction Stir Welding for Aluminum Alloy Circumferential Weld Application," *ASM Aeromat 2003*, 2003.
- [4] S. B. Aziz, M. W. Dewan, D. J. Huggett, M. A. Wahab, A. M. Okeil and T. W. Liao, "A fully coupled thermomechanical model of friction stir welding (FSW) and numerical studies on process parameters of lightweight aluminum alloy joints," *Acta Metallurgica Sinica (English Letters)*, vol. 31, no. 1, pp. 1-18, 1 2018.
- [5] X. Liu, G. Chen, J. Ni and Z. Feng, "Computational Fluid Dynamics Modeling on Steady-State Friction Stir Welding of Aluminum Alloy 6061 to TRIP Steel," *Journal of Manufacturing Science and Engineering, Transactions of the ASME*, vol. 139, no. 5, 5 2017.
- [6] C. Zhao and X. Liu, "Computational Analysis on Weld Formation Mechanism during Self-Reacting Friction Stir Welding," *Journal of Manufacturing Science and Engineering*, pp. 1-15, 10 2020.
- [7] T. Sheppard and D. Wright, "Determination of flow stress: Part 1 constitutive equation for aluminium alloys at elevated temperatures," *Metals Technology*, vol. 6, no. 1, pp. 215-223, 1979.
- [8] C. Zhao, X. Pei and X. Liu, "Computational investigation on void defects formation and periodic tool-workpiece sliding-to-sticking transition in self-reacting friction stir welding," *International Journal of Advanced Manufacturing Technology*, vol. 120, no. 11-12, pp. 8075-8088, 6 2022.
- [9] D. Prymak, M. Miles, T. Nelson and F. Michael, "A high-pressure shear testing approach to measure flow stresses near a friction stir welding tool," *Materials Performance and Characterization*, vol. 10, no. 1, pp. 727-738, 10 2021.
- [10] K. Kuykendall, T. Nelson and C. Sorensen, "On the selection of constitutive laws used in modeling friction stir welding," *International Journal of Machine Tools and Manufacture*, vol. 74, pp. 74-85, 2013.
- [11] K. Kuykendall, "An Evaluation of Constitutive Laws and their Ability to Predict Flow Stress over Large Variations in Temperature, Strain, and Strain Rate Characteristic of Friction Stir Welding," 2011.
- [12] U. Reisgen, A. Schiebahn, R. Sharma, A. Maslennikov, P. Rabe and V. Erofeev, "A method for evaluating dynamic viscosity of alloys during friction stir welding," *Journal of Advanced Joining Processes*, vol. 1, 3 2020.

- [13] H. He, Y. Yi, J. Cui and S. Huang, "Hot deformation characteristics and processing parameter optimization of 2219 Al alloy using constitutive equation and processing map," *Vacuum*, vol. 160, pp. 293-302, 2 2019.
- [14] S. N. Murty, A. Sarkar, P. R. Narayanan,, P. Venkitakrishnan, and J. Mukhopadhyay, "Development of processing maps and constitutive relationship for thermomechanical processing of aluminum alloy AA2219," *Journal of Materials Engineering and Performance*, vol. 26, pp. 2190-2203, 2017.
- [15] L. LIU, Y. x. WU, H. GONG and K. WANG, "Modification of constitutive model and evolution of activation energy on 2219 aluminum alloy during warm deformation process," *Transactions of Nonferrous Metals Society of China (English Edition)*, vol. 29, no. 3, pp. 448-459, 3 2019.
- [16] L. Liu, Y. Wu, H. Gong, S. Li and A. S. Ahmad, "A physically based constitutive model and continuous dynamic recrystallization behavior analysis of 2219 aluminum alloy during hot deformation process," *Materials*, vol. 11, no. 8, 8 2018.
- [17] K. E. Tello, A. P. Gerlich and P. F. Mendez, "Constants for hot deformation constitutive models for recent experimental data," *Science and Technology of Welding and Joining*, vol. 15, no. 3, pp. 260-266, 4 2010.
- [18] H. Wang, G. Qin and C. Li, "A modified Arrhenius constitutive model of 2219-O aluminum alloy based on hot compression with simulation verification," *Journal of Materials Research and Technology*, vol. 19, pp. 3302-3320, 2022.
- [19] A. Gilmore and X. Liu, "Mechanical Behavior and Microstructure Evolution during Hot Torsion Deformation of Aluminum Alloy AA2219," *Advanced Engineering Materials*, 2022.
- [20] S. B. Aziz, M. W. Dewan, D. J. Huggett, M. A. Wahab, A. M. Okeil and T. W. Liao, "Impact of Friction Stir Welding (FSW) process parameters on thermal modeling and heat generation of aluminum alloy joints," *Acta Metallurgica Sinica (English Letters)*, vol. 29, no. 9, pp. 869-883, 9 2016.
- [21] B. C. Liechty and B. W. Webb, "Modeling the frictional boundary condition in friction stir welding," *International Journal of Machine Tools and Manufacture*, vol. 48, no. 12-13, pp. 1474-1485, 10 2008.
- [22] Q. Liu, W. Li, L. Zhu, Y. Gao, L. Xing, Y. Duan and L. Ke, "Temperature-dependent friction coefficient and its effect on modeling friction stir welding for aluminum alloys," *Journal of Manufacturing Processes*, vol. 84, pp. 1054-1063, 12 2022.
- [23] C. K. Lieou and C. A. Bronkhorst, "Thermomechanical conversion in metals: dislocation plasticity model evaluation of the Taylor-Quinney coefficient," *Acta Materialia*, vol. 202, pp. 170-180, 1 2021.
- [24] T. Jiang, C. Wu and H. Su, "Determination of self-adaptive slip rate at tool/workpiece interface in numerical model of friction stir welding," *Materials Today Communication*, vol. 33, p. 104428, 2022.

- [25] A. Zhang and Y. Li, "Thermal Conductivity of Aluminum Alloys—A Review," *Materials*, vol. 16, no. 8, 4 2023.
- [26] X. Lu, Y. Luan, X. Meng, Y. Zhou, N. Zhao and S. Y. Liang, "Temperature Distribution And Mechanical Properties of FSW Medium Thickness 2219 Aluminum Alloy," *The International Journal of Advanced Manufacturing Technology*, 2022.
- [27] Ansys, Inc. , "Ansys Fluent User's Guide," Ansys, Inc., 2023.
- [28] Ansys, Inc., "Ansys Fluent Customization Manual," Ansys, Inc., 2023.
- [29] H. R. Shercliff, M. J. Russell, A. Taylor and T. L. Dickerson, "Microstructural modelling in friction stir welding of 2000 series aluminium alloys," *Mecanique et Industries*, vol. 6, no. 1, pp. 25-35, 1 2005.
- [30] Ansys, Inc., "Ansys Fluent Theory Guide," Ansys, Inc., 2023.
- [31] L. Wu and W. G. Ferguson, "Modelling of Precipitation Hardening in Casting Aluminium Alloys," *Aluminium alloys, theory and applications*, pp. 307-330, 2011.
- [32] S. N. Samaras, "Modelling of microstructure evolution during precipitation processes: A population balance approach of the KWN model," *Modelling and Simulation in Materials Science and Engineering*, vol. 14, no. 8, pp. 1271-1292, 12 2006.
- [33] D. J. Prymak, "A New Method of Measuring Flow Stress for Improved Modeling A New Method of Measuring Flow Stress for Improved Modeling of Friction Stir Welding of Friction Stir Welding," 2021.